



# Spectroscopy and Structure of the Simplest Actinide Bonds

Michael C. Heaven\*

Department of Chemistry, Emory University, Atlanta, Georgia 30322, United States

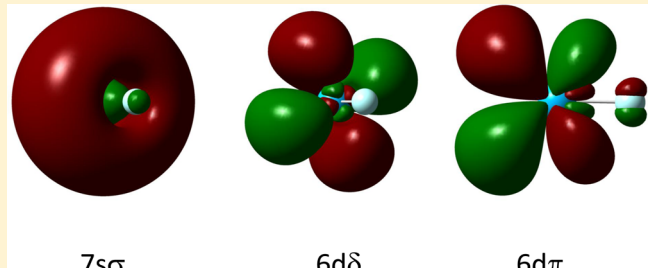
Beau J. Barker

Chemistry Division, Los Alamos National Laboratory, Los Alamos, New Mexico 87545, United States

Ivan O. Antonov

Combustion Research Facility, Sandia National Laboratory, Livermore, California 94550, United States

**ABSTRACT:** Understanding the influence of electrons in partially filled f- and d-orbitals on bonding and reactivity is a key issue for actinide chemistry. This question can be investigated by using a combination of well-defined experimental measurements and theoretical calculations. Gas phase spectroscopic data are particularly valuable for the evaluation of theoretical models. Consequently, the primary objectives of our research have been to obtain gas phase spectra for small actinide molecules. To complement the experimental effort, we are investigating the potential for using relativistic ab initio calculations and semiempirical models to predict and interpret the electronic energy level patterns for f-element compounds. Multiple resonance spectroscopy and jet cooling techniques have been used to unravel the complex electronic spectra of Th and U compounds. Recent results for fluorides, sulfides, and nitrides are discussed.



7s $\sigma$

6d $\delta$

6d $\pi$

## INTRODUCTION

Studies of the bonding and electronic structures of simple actinide compounds are of interest from both practical and theoretical perspectives.<sup>1</sup> Starting with the practical issues, the propensity for actinides to undergo nuclear fission is widely exploited in weapons and nuclear power generation. However, the radioactive decay processes also pose significant technological problems for the safe treatment and long-term storage of spent nuclear materials. A notable example of the waste handling problem is presented by the legacy from the Manhattan project. This includes billions of gallons of radiologically contaminated liquid waste.<sup>2</sup> Cost effective extraction of the actinides is the key first step in the remediation of this material, but the appropriate chemical means have yet to be determined. At present, our understanding of the chemistry of the actinides is limited as compared to the situation for d-block transition metals or the lanthanides. This is because most actinides were discovered relatively recently, the radioactive species are difficult to work with, and many have short lifetimes.

Given these circumstances, the practical motivation for theoretical investigations of actinides are readily apparent. Computational methods could provide safe and low-cost methodologies for the exploration of actinide chemistry. Ideally, this would be carried out using first-principles quantum mechanical methods (e.g., ab initio electronic structure calculations). In recent years the advances made in using

computational methods to predict the properties and reaction pathways for compounds of first and second row elements have been remarkable. Extensions of these techniques to compounds that contain transition metals has also been impressive, but the difficulties mount as the atomic number ( $Z$ ) increases. Problems arise from the number of electrons that must be considered and the need to account for relativistic effects. The latter include the velocity dependence of the electron mass (resulting from the high velocity achieved when an electron approaches a high- $Z$  nucleus) and strong spin–orbit effects. At present, all-electron relativistic quantum chemistry calculations for actinide-containing species are impractical for all but the simplest molecules. Several strategies are being developed to address this challenge. A critical step has been the development of effective core potentials (ECP's) for the actinides.<sup>3–5</sup> This method uses simplified functions to represent the behavior of a subset of core electrons, with the relativistic effects folded in. The computational effort can then be focused on the valence electrons.

Even with the use of ECP's, ab initio calculations for larger actinide containing molecules, and actinides in condensed phases, are often found to be impractically demanding. Consequently, density functional theory (DFT), which is far

Received: July 21, 2014

Revised: September 16, 2014

Published: September 22, 2014



more computationally efficient, has been a heavily used tool for computational studies of actinide chemistry. In addition, molecular mechanics methods are currently being developed for the design and evaluation of actinide-specific chelating ligands,<sup>6</sup> a task where very rapid computation is required to permit comparisons of large numbers of complex structures. The force-fields used in these calculations are, in part, constructed using the results from electronic structures calculations.

From the perspective of fundamental scientific significance, studies of small actinide-containing molecules provide opportunities to evaluate and advance relativistic quantum chemistry models.<sup>7–12</sup> Central issues for the actinides concern the participation of the 5f orbitals in chemical bonding,<sup>13</sup> and the unique materials properties that result from the partially filled 5f shell (e.g., superconductivity, heavy-Fermion behavior and single-molecule magnets). Comparisons between the lanthanides and the actinides are complicated by substantial differences in the radial distributions of the 4f and 5f orbitals. The 4f orbitals are very compact, and the electrons in these atomic-like orbitals have minimal participation in bonding interactions. The 5f orbitals of the actinides are not so strongly contracted and are at energies close to those of the 7s and 6d orbitals. As a consequence, the 5f electrons of the early actinides do appear to participate in bonding under favorable circumstances. As the 5f orbitals contract with increasing  $Z$ , it is expected that the later actinides will be more lanthanide-like in their behavior. These inferences are derived from theoretical models that require validation using a variety of spectroscopic observations.

The electronically excited states of actinide species are often at low enough energies that they must be included in thermodynamic calculations. For example, the first electronically excited states of UO and  $\text{UO}_2$  are found at 294 and 360  $\text{cm}^{-1}$ , respectively.<sup>14,15</sup> As calculations for excited states of actinides are particularly challenging, ligand field theory (LFT) models have often been used to interpret spectroscopic data. LFT is known to work well for the lanthanides,<sup>16</sup> as would be expected given the compactness of their 4f orbitals. The basis for the application of LFT to actinides, with their larger radius 5f orbitals, is less secure. However, as the techniques for obtaining definitive spectra and high-level theoretical predictions advance, the questionable applicability of LFT for the actinides can be turned to some advantage. Deviations from the LFT predicted energy levels can be used to gauge the degree to which the 5f electrons participate in the bonding.

Simple actinide molecules are also proving to be useful for experiments designed to test extensions to the standard model of particle physics. In particular, the diatomics  $\text{ThO}$  and  $\text{ThF}^+$  have been identified as species that are suitable for investigation of the electron electric dipole moment (eEDM), which results from a charge-parity symmetry violation.<sup>17–20</sup> Extensions to the standard model have many orders of magnitude differences in their predictions for the eEDM. The experimental value has yet to be determined, but measurements that reduce the upper bound yield critical constraints. As the eEDM is very small (the current upper bound is  $|\mu_e| < 8.7 \times 10^{-29} \text{ e cm}$ ), it is a challenge to identify unambiguous manifestations of its presence. The present strategy is to exploit the extremely high internal electric fields that can be generated in ionic diatomic molecules. The most promising candidates are molecules that have a nucleus that carries a high charge. For reasons that are associated with the minimization of magnetic moment effects and the ability to

polarize the molecule using a modest external electric field, molecules that have an accessible, long-lived  ${}^3\Delta_1$  electronic state are the most favorable.<sup>21</sup> Both  $\text{ThO}$  and  $\text{ThF}^+$  have such states, and theoretical calculations indicate the internal fields in excess of 80 GV/cm can be attained in these molecules.<sup>17</sup>  $\text{ThO}$  was used in the most recent determination of the eEDM upper bound.<sup>17</sup> The high density of low-lying electronic states for actinide diatomics is also of interest for experiments that explore time variations of fundamental constants.<sup>22</sup>

The research described in this article has been focused on spectroscopic and theoretical studies of diatomic molecules that contain Th and U. Some discussion of related Hf species has been included, as the comparisons between isoelectronic Hf and Th compounds yield useful insights. The spectroscopic studies have been conducted in the gas phase, to obtain results that can be compared directly with theoretical calculations for isolated molecules. The data are not complicated by solvent effects or interactions with counterions. Another advantage of gas phase spectroscopy is that it can yield unambiguous assignments for the states that are being observed. This minimizes the bias that can be built-in when theoretical calculations are first used to assign spectra, which are then, in turn, used to evaluate the theoretical predictions.

At this point a clarification of the title for this article is appropriate. Diatomics are the simplest molecules in terms of the number of nuclei involved and geometry, but they are not necessarily the simplest in terms of electronic structure. For example,  $\text{ThO}_2$  and  $\text{UO}_3$  are closed-shell ionic molecules with ground states that are well-removed from the first electronically excited states. In contrast, the lowest energy configuration of UO is  $\text{U}^{2+}(5f^67s)\text{O}^{2-}$ , with the  $\text{U}^{2+}(5f^67s^2)\text{O}^{2-}$  configuration at a very slightly higher energy. These two configurations give rise to a total of 819 bound states.<sup>14</sup> Clearly, the low-energy electronic complexity of UO far exceeds that of  $\text{ThO}_2$  or  $\text{UO}_3$ . The upside of the electronic complexity for the diatomics is that it provides opportunities to observe the behavior of the 5f electrons in the lowest energy states, which are the most accessible to high-level theoretical analyses.

The spectroscopic techniques used in our research, and previous studies of  $\text{ThO}$ , UO, and  $\text{UO}_2$ , have been the subject of a review article in 2006<sup>23</sup> and a book chapter published in 2010.<sup>24</sup> The present article covers recent progress for the molecules  $\text{UF}/\text{UF}^+$  and  $\text{ThX}/\text{ThX}^+$  ( $X = \text{F}, \text{N}, \text{S}$ ), with some discussion of the previous work to make this a nearly self-contained account.

## ■ EXPERIMENTAL TECHNIQUES

Many of the actinide species of interest are refractory materials that have high melting points. High temperatures are needed to obtain gas phase samples at sufficiently high number densities for spectroscopic experiments. For example, our early studies of the electronic spectroscopy of UO were conducted using a tube furnace that was heated to a temperature of 2400 K.<sup>14</sup> Apart from the materials problems posed by such experiments, the high temperature hampers spectroscopic measurements. A large number of ro-vibronic states are populated, resulting in excessive spectral congestion and low number densities per quantum state. The solution to this problem has been to use pulsed laser vaporization to entrain the metal vapor in a supersonic expansion (usually driven by He or Ar carrier gas).<sup>23</sup> Reactants can be introduced as a trace component of the carrier gas, permitting kinetically limited chemistry to occur prior to supersonic expansion and cooling. Using this approach, gas

phase samples of molecules such as UO and UF have been produced with internal temperatures as low as 10 K.

Pulsed production of cold molecules can be combined with a wide range of different spectroscopic observation techniques. The spectrometer developed for our actinide experiments allows for observations using laser-induced fluorescence (LIF), dispersed fluorescence (DF), resonantly enhanced multiphoton ionization (REMPI), photoionization efficiency (PIE), and pulsed-field ionization zero kinetic energy (PFI-ZEKE) photoelectron spectroscopy. The main features of the spectrometer are shown in Figure 1. This apparatus consists of two

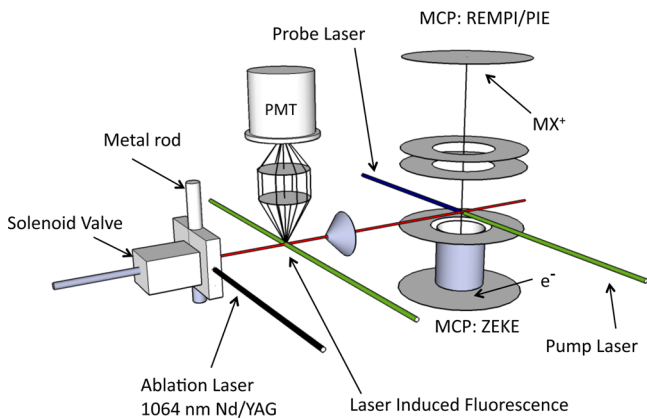


**Figure 1.** Schematic diagram of the apparatus used to record REMPI, PIE, and PFI-ZEKE spectra for actinide containing molecules.

differentially pumped vacuum chambers. The first, shown on the left-hand side, houses the laser vaporization source and the components used for LIF detection. Dispersed fluorescence spectra are recorded by inserting a monochromator in front of the photomultiplier.

A conical skimmer is used to transmit the core of the jet expansion into the second vacuum chamber, which houses the components for cation and electron detection. Typically, two laser photons are used to induce ionization via an electronically excited state of the molecule. For REMPI spectroscopy the energy of the first photon is swept, and the energy of the second photon is sufficient to ionize the excited molecules, but not those in the ground state. A time-of-flight mass spectrometer is used for mass selective detection of the ions (upward path in Figure 1). Both LIF and REMPI techniques yield information concerning the electronic states of the neutral molecule.

Ionization processes are characterized with the first laser pulse tuned to an electronic transition of the neutral molecule, and the energy of the second photon tuned through the range that will access (via the sum of photon energies) the ionization threshold of interest. With detection of the resulting cations (PIE spectrum), this method can be used to locate the first ionization threshold with reasonable accuracy (errors on the order of 30  $\text{cm}^{-1}$ ). Scanning to energies above the first threshold often yields a highly structured PIE trace that is dominated by autoionizing resonances. These resonances obscure features that might be used to extract spectroscopic data for the molecular cation, but they can be greatly diminished by the use of the PFI-ZEKE technique.<sup>25</sup> Here, the two photons are used to excite the molecule to a long-lived, high- $n$  Rydberg state that lies just below a bound state of the ion. Excitation takes place under field-free conditions and the

electrons produced by autoionizing processes drift away from the detection region. After a suitable delay (on the order of microseconds), a weak pulsed electric field is used to ionize the molecules that were trapped in Rydberg states. The same field accelerates the electrons toward a microchannel plate for detection (lower MCP in Figure 1). The spectra obtained by this means yield molecular constants for the ions.

To illustrate the advantage of using the PFI-ZEKE method, Figure 2 shows a comparison of PIE and PFI-ZEKE spectra for

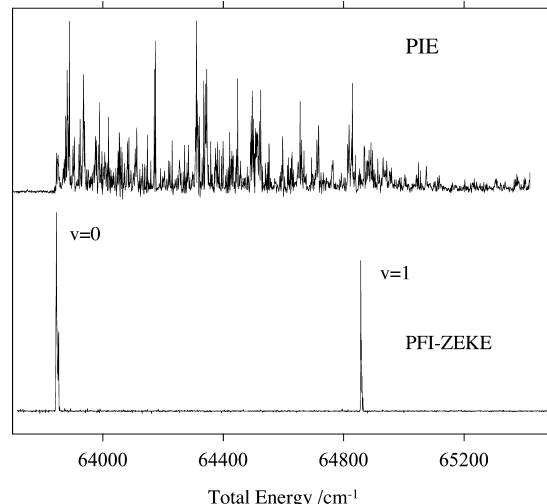


**Figure 2.** Two-color PIE and PFI-ZEKE spectra for HfO. The upper trace, which shows the PIE spectrum, is dominated by closely spaced autoionizing features. The loss of intensity on the high-energy side of the spectrum is due to the wavelength dependence of the dye laser power. The lower trace shows the PFI-ZEKE spectrum, where the states of the HfO<sup>+</sup> ion are cleanly separated from the autoionizing resonances.

HfO.<sup>26</sup> In the upper trace, the congested and irregular structure of the PIE scan results from the many series of Rydberg energy levels that converge to the various ro-vibrational levels of HfO X(1) $^2\Sigma^+$ . Electrons from the autoionizing resonances are allowed to dissipate before the detection field is applied in the PFI-ZEKE experiment, so the spectrum prominently displays the near threshold states (those within 2  $\text{cm}^{-1}$  of the limit). As can be seen in the lower trace of Figure 2, this provides a clean vibrationally resolved spectrum for the ion. For metal oxides and fluorides the resolution is sufficient to show the rotational structure associated with each vibronic level (not shown in Figure 2 but easily achieved for HfO<sup>+</sup> (see Figure 7 of ref 26)). Beyond determination of the rotational constant and bond length, observation of the rotational structure proves to be critical for determination of the electronic angular momentum of the state.

**Spectroscopic and Theoretical Studies of UF and UF<sup>+</sup>.** In discussing recent work on UF and UF<sup>+</sup>, it is helpful to begin with some preliminary comments concerning the electronic structures observed for UO and UO<sup>+</sup>. Considered in terms of a formal LFT framework, UO and UF<sup>+</sup> are related as they are expected to share a common U<sup>2+</sup>(5f<sup>3</sup>7s) atomic ion core, perturbed by a closed-shell O<sup>2-</sup> or F<sup>-</sup> anion. The UO<sup>+</sup> ion and neutral UF are also comparable because the electronic complexity in both molecules arises from the 5f<sup>3</sup> configuration (U<sup>3+</sup>(5f<sup>3</sup>)O<sup>2-</sup> and U<sup>+(5f<sup>3</sup>7s<sup>2</sup>)F<sup>-</sup>).</sup>

PFI-ZEKE spectra confirmed that the ground state of  $\text{UO}^+$  has  $|\Omega| = 4.5$  and is derived from the  $\text{U}^{3+}(5f^3, ^4\text{I}_{4,5})$  configuration.<sup>27</sup> The notation used here specifies the Russell–Saunders atomic term symbol for the metal ion,  ${}^{2S+1}L_{J_a}$  where  $S$  is the spin,  $L$  is the electronic orbital angular momentum, and  $J_a$  is the total electronic angular momentum (the subscript  $a$  indicates that this is an atomic ion property). In the diatomic molecule, the unsigned projection of  $J_a$  on the diatomic axis, denoted by  $|\Omega|$ , is a well-defined quantum number. For a less than half-filled subshell, the highest projection of  $J_a$  gives the lowest energy state. Hence, the  $J_a = 4.5$  atomic core produces an ascending tier of molecular states with  $|\Omega| = 4.5, 3.5, 2.5, 1.5$ , and 0.5. Above this manifold the  ${}^4\text{I}_{5,5}$  core produces states with  $|\Omega| = 5.5–0.5$ . Note that the bonding is primarily ionic, so that spin–orbit excitation and rotation of the  $J_a$  vector have only modest effects on the vibrational and rotational constants. As noted by Field<sup>16</sup> for the lanthanides, the molecular constants can be characteristic of the parent ion configuration. For example, the states of  $\text{UO}^+$  derived from the  ${}^4\text{I}_{4,5}$  core exhibit vibrational constants that span the range from 911.9 to 905.2  $\text{cm}^{-1}$ . Furthermore, the atomic  ${}^4\text{I}_{5,5}–{}^4\text{I}_{4,5}$  spin–orbit energy interval of  $\text{U}^{3+}$  was replicated multiple times by the low-energy states of  $\text{UO}^+$ . This suggests that the 5f orbitals have retained their atomic character and do not participate significantly in the formation of the U–O bond.<sup>27</sup>

Prior to our recent study,<sup>28</sup> there were no spectroscopic data available for UF or  $\text{UF}^+$ . Gas phase UF was generated using the reaction of the metal vapor with  $\text{SF}_6$ . LIF and REMPI spectra recorded for the 18 000–20 000  $\text{cm}^{-1}$  range contained several bands of UF. Figure 3 shows the rotational structure of a band

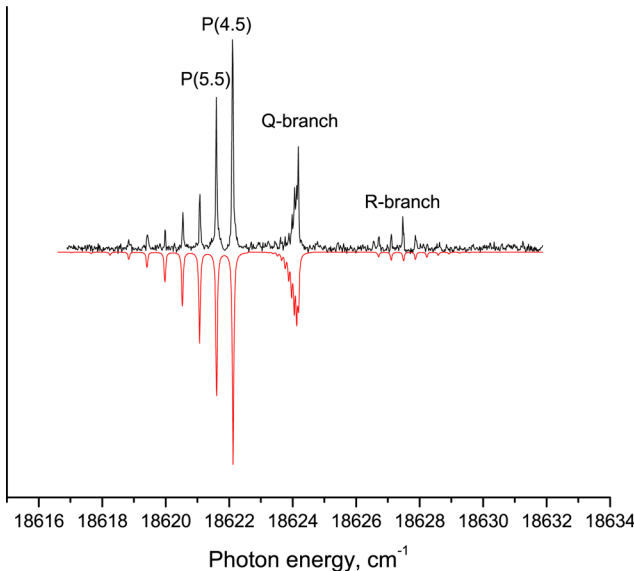


**Figure 3.** Laser-induced fluorescence spectrum of the [18.6]3.5-X(1)4.5 transition of UF. The black trace is the experimental data, and the red trace (inverted) is a computational simulation. The rotational temperature was set to 9 K.

centered at 18 624  $\text{cm}^{-1}$ . An important feature of this spectrum is that the first lines observed in the P- and R-branches are for  $J = 4.5$ , where  $J$  is the total angular momentum including molecular rotation (but not the nuclear spin). As the total angular momentum cannot be less than its body-fixed projection, the first lines uniquely identify the upper and lower state  $|\Omega|$  values as 3.5 and 4.5, respectively. This was

consistent with the prediction of an  $|\Omega| = 4.5$  ground state by both LFT and ab initio electronic structure calculations. A DF spectrum, recorded using excitation of the 18 624  $\text{cm}^{-1}$  band, showed the presence of two low-lying electronic states, tentatively identified as the  $|\Omega| = 3.5$  ( $T_0 = 435 \text{ cm}^{-1}$ ) and 2.5 ( $T_0 = 650 \text{ cm}^{-1}$ ) components of  $\text{U}^+(5f^37s^2, {}^4\text{I}_{4,5})\text{F}^-$ . Despite the presence of several other low-lying states, those that could be observed were limited by the  $\Delta|\Omega| = 0, \pm 1$  optical selection rule.

Theoretical studies of UF have been carried out using ECP's,<sup>29</sup> all-electron basis sets,<sup>30,31</sup> and DFT.<sup>32</sup> An early ECP study by Krauss and Stevens<sup>29</sup> assumed that the ground state would be derived from the high-spin  $\text{U}^+(5f^36d7s)\text{F}^-$  configuration. This yielded many low-lying states and the conclusion that the 5f electrons did not participate in the bonding. Subsequently, the all-electron relativistic calculations of Fedorov et al.<sup>30</sup> found the lowest energy configuration to be  $\text{U}^+(5f^37s^2)\text{F}^-$ . Spin–orbit coupling was included in this study, and the calculated pattern of low-lying states was consistent with the electrostatic LFT picture presented above. The first state belonging to the 5f<sup>3</sup>6d7s configuration ( ${}^6\Lambda_{5,5}$ ) was predicted at 7357  $\text{cm}^{-1}$ .

For a more detailed comparison with the experimental results, Antonov and Heaven<sup>28</sup> computed the low-energy states using the CASSCF/CASPT2 method with a small core ECP for U (60 e core).<sup>33</sup> For the electrons treated explicitly, a (14s13p10d8f6g)/[6s6p5d4f3g] ANO contracted basis set was centered on the U atom,<sup>33</sup> and the aug-cc-pVTZ Dunning correlation consistent basis set was used for the F atom.<sup>34</sup> Spin–orbit interaction energies were calculated using the Breit–Pauli Hamiltonian with the CASSCF wave functions.<sup>35</sup> The pattern of low-lying states was again consistent with LFT expectations and the results of Fedorov et al.,<sup>30</sup> with predictions for the term energies of the  $|\Omega| = 3.5$  and 2.5 states that were somewhat improved. Near the equilibrium distance the ground state wave function was almost entirely of 5f<sup>3</sup>7s<sup>2</sup> character, with leading spin–orbit contributions of 80.74%  ${}^4\text{I}_{4,5} + 16.50\% {}^4\text{H}_{4,5} + 2.54\% {}^4\Gamma_{4,5} + 0.22\% {}^4\Phi_{4,5}$ . The permanent electric dipole moment, calculated for an internuclear distance of 2.0 Å, was 1.99 D.

Linton et al.<sup>36</sup> have recently tested the predictions for UF X(1)4.5 by using the Stark and Zeeman effects to measure the dipole moment (2.01(1) D) and magnetic g-factor (3.28(1)). The theoretical value for the latter, derived from the wave function decomposition given above, was 3.22. Hence, the CASPT2 results were found to be in good agreement with the experimental data.

PFI-ZEKE spectroscopy was used to map the low-energy states of the  $\text{UF}^+$  cation. The transition at 18 624  $\text{cm}^{-1}$  (Figure 3) was used for the first excitation step. Figure 4 shows the vibronic structure of  $\text{UF}^+$ . For each value of  $|\Omega|$ , long vibrational progressions were observed (for almost all bands the  $|\Omega|$  assignments were uniquely determined from the rotational structures). A curious feature of the PFI-ZEKE spectrum is that the vibronic intensities do not appear to follow the Franck–Condon principle. The changes in the equilibrium distances between the intermediate excited state of UF and the low-energy states of  $\text{UF}^+$  are quite small. Transitions to the  $v = 0$  levels of the ion would be expected to dominate, but this was not observed. We have noted this behavior for several metal oxide species when two-color excitation is employed.<sup>23,37</sup> It seems likely that state mixing of the electronically excited states

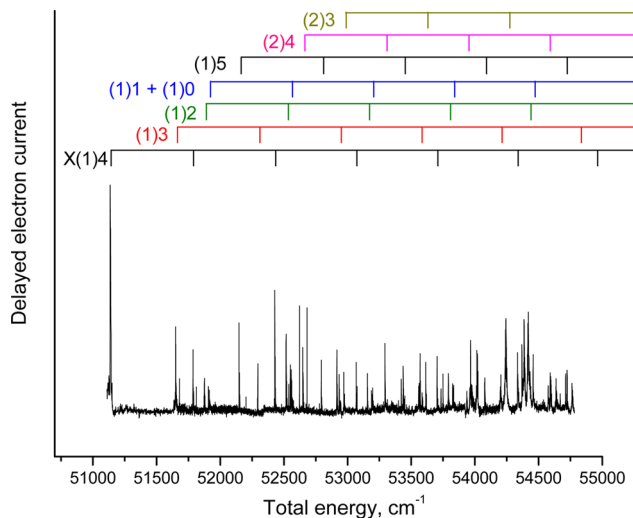


**Figure 4.** Two-color PFI-ZEKE survey scan of  $\text{UF}^+$ . The horizontal axis is the sum of the energies of two photons.

of the neutral molecule causes departure from the simple Franck–Condon overlap model.

The relaxed selection rules for the PFI-ZEKE transitions greatly facilitate the process of finding characteristic patterns among the low-energy states. Excitation of the high- $n$  Rydberg states provides access to final states with no restriction on the overall change in  $|\Omega|$ . Hence, all states arising from a given atomic ion configuration can be located. For  $\text{UF}^+$ , all  $|\Omega|$  components of the  $\text{U}^{2+}(5\text{f}^3[4\text{I}]7\text{s})$   $J_a = 4$  and 5 configurations were characterized, along with two states from  $J_a = 6$ . The electronic term energies and tightly clustered vibrational constants ( $\sim 649 \text{ cm}^{-1}$ ) were consistent with LFT expectations. This point is illustrated in Figure 5, where the  $\text{UF}^+$  term energies are compared with those of  $\text{UO}$  and the results from ab initio electronic structure calculations (CASSCF/CASPT2/spin-orbit) for  $\text{UF}^+$  and  $\text{U}^{2+}$ .

To link the  $\text{UF}^+$  electronic structure to the parent atomic ion states, the energies of the  $\text{U}^{2+}$  free-ion  $J_a = 4, 5, 6$ , and 5 levels

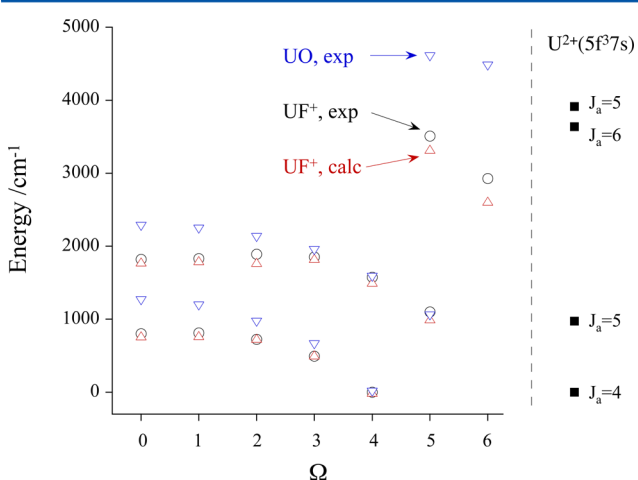


**Figure 5.** Energy level diagram of  $\text{UF}^+$  and  $\text{UO}$  electronic states. The open black circles are the  $\text{UF}^+$  experimental data, red upward-pointing triangles are the calculated energies, and the blue downward-pointing triangles are  $\text{UO}$  experimental data. The filled squares on the right-hand side are the calculated energies of the lowest levels of the  $\text{U}^{2+}$   $\text{f}^3$  configuration relative to the lowest  $\text{f}^3$   $J_a = 4$  level.

are indicated by the filled black squares in Figure 5. The observed and calculated energy levels of  $\text{UF}^+$  are represented by the open circles and upward-pointing red triangles, respectively. It is evident that the energy levels are consistent with the projection states of  $J_a = 4, 5$ , and 6. Note that the intervals between the  $J_a = 4, |\Omega|$  and  $J_a = 5, |\Omega| + 1$  states are close to the that of the atomic ion limit. The  $\text{UF}^+$  states observed for  $J_a = 6$  are somewhat below the free ion energy, which is indicative of a slight quenching of the spin-orbit interaction energy for the  $5\text{f}^3$  electrons. All of these trends were recovered by the CASSCF/CASPT2/SO calculations.

As a further demonstration of the applicability of LFT for ionic  $\text{U}-\text{X}$  bonds, Figure 5 includes the energy levels of  $\text{UO}$ ,<sup>14,38</sup> which are shown as downward-pointing blue triangles. The  $J_a = 4$  and 5 manifolds follow the expected trends. The states with the highest projections of  $J_a$  have very similar energies for  $\text{UF}^+$  and  $\text{UO}$ . As the  $J_a$  vector is rotated away from the internuclear axis, the energies of the  $\text{UO}$  state increase more rapidly than those of  $\text{UF}^+$ . This is a simple consequence of the stronger ligand field of  $\text{UO}$  resulting from the shorter bond length and greater charge separation (the dipole moment for the ground state of  $\text{UO}$  is  $3.363(26) \text{ D}^{39}$ ). The only observed  $|\Omega| = 6$  state for  $\text{UO}$  is above the free-ion  $J_a = 6$  level. Interpretation of this observation is complicated by the fact that the states for  $5\text{f}^27\text{s}$  and  $5\text{f}^27\text{s}^2$  are interleaved and mutually perturbing.<sup>14</sup> Due to the weaker field of  $\text{UF}^+$  the  $5\text{f}^27\text{s}$  configuration is not as strongly destabilized relative to  $5\text{f}^27\text{s}^2$ . Consequently, the lowest energy  $5\text{f}^27\text{s}^2$  state of  $\text{UF}^+$  is  $2593 \text{ cm}^{-1}$  above the ground state.

Previous electron impact ionization measurements for  $\text{UF}$  had provided an estimate for the IE of  $6.0(3) \text{ eV}$ .<sup>40</sup> The PFI-ZEKE measurement gave  $6.34159(6) \text{ eV}$ , which is  $0.148 \text{ eV}$  greater than that of atomic  $\text{U}$ . This shows that removal of the  $7\text{s}$  electron slightly reduced the strength of the bonding, consistent with the notion that this is a metal-centered nonbonding orbital.

**Ligand Field Theory for the Low-Energy States of  $\text{UF}$ ,  $\text{UO}^+$ , and  $\text{UN}$ .** Although the data available for the low-energy states of  $\text{UF}$  are sparse,<sup>28</sup> it appears that they are formally consistent with the perturbation of the  $\text{U}^+(5\text{f}^3[4\text{I}_{4,5}]7\text{s}^2)$  ion by the field of the  $\text{F}^-$  ligand. The comparison to  $\text{UO}^+$ , where the  $\text{U}^{3+}(5\text{f}^3[4\text{I}_{4,5}])$  ion is perturbed by closed-shell  $\text{O}^{2-}$ , shows that the electrostatic perturbation in the oxide ion is substantially greater. Table 1 lists the relevant energy levels for  $\text{UF}$  (observed and calculated) and  $\text{UO}^+$ . Here it can be seen that the energy range spanned by the  $J_a = 4.5$  states is a factor of approximately 1.7 times greater for  $\text{UO}^+$ , due to the larger internal field. As  $\text{UN}$  is isoelectronic  $\text{UO}^+$ , it seems reasonable to expect the same pattern of low-lying states arising from the

**Table 1. Comparison of Experimental and Theoretical Excitation Energies of Low-Lying Electronic States of  $\text{UF}$  and  $\text{UO}^+{}^a$**

state	UF, theory <sup>b</sup>	UF, theory <sup>c</sup>	UF, exp	$\text{UO}^+$ , exp <sup>d</sup>
X(1)4.5	0	0	0	0
(1)3.5	415	61	435	764.93
(1)2.5	678	805	650	1132.42
(1)1.5	824	944		1284.50
(1)0.5	790	794		1324.9

<sup>a</sup>All energies given in units of  $\text{cm}^{-1}$ . <sup>b</sup>Single-point calculations at  $R = 2.00 \text{ \AA}$ . <sup>c</sup>Data from Fedorov et al.<sup>30</sup> <sup>d</sup>Data from Goncharov et al.<sup>27</sup>

$^4I_{4,5}$  free-ion. However, Matthew and Morse<sup>41</sup> recently obtained the first gas phase spectra for UN, and their data show definitively that the ground state has  $|\Omega| = 3.5$ . They accounted for this observation by noting that the bond length for UN X(1)3.5 (1.764 Å) is shorter than that of UO<sup>+</sup> X(1)4.5 (1.807 Å), and that the internal field is larger. The electrostatic destabilization of the  $5f^3$  configuration in UN is sufficient to push it above  $5f^27s$ , which gives rise to the U( $5f^27s, ^4H_{3,5}$ )N X(1)3.5 ground state. Several electronically excited states of UN were characterized by Matthew and Morse<sup>41</sup> using REMPI spectroscopy at the level of rotational resolution. In future studies of this molecule it will be of interest to examine the low-energy states, to probe the energy spacing between  $5f^3$  and  $5f^27s$  configurations.

**Spectroscopic and Theoretical Studies of ThF and ThF<sup>+</sup>.** A significant difference between Th and U is that the 5f orbitals of Th are appreciably above the 6d orbitals.<sup>42</sup> This simplifies the low-energy electronic structure for ThX diatomics, as compared to the corresponding U and transuranic AnX species. Spectroscopic data for ThX species consist of matrix isolation IR measurements of vibrational fundamentals (ThO,<sup>43</sup> ThN,<sup>44</sup> ThH<sup>45</sup>) and gas phase spectra for ThO/ThO<sup>+</sup> (refs 18, 19, and 46–57) ThS/ThS and ThF/ThF<sup>+</sup> (ref 58). ThO is the most heavily studied of these diatomics and has been the focus of recent attempts to measure the eEDM.<sup>19</sup>

Although the 7s and 6d orbitals of Th are available for covalent bonding, the low-energy states of the ionically bound molecules are readily anticipated using LFT.<sup>14,57</sup> For example, ThO exhibits a Th<sup>2+</sup>(7s<sup>2</sup>)O<sup>2-</sup> X(1) $\Sigma^+$  ground state with low-lying states ((1) $^3\Delta$ , (1) $^3\Pi$ , (1) $^3\Sigma^+$ ) derived from the Th<sup>2+</sup>(7s6d)O<sup>2-</sup> configuration.<sup>14,57</sup> Similarly, the cation has a Th<sup>3+</sup>(7s)O<sup>2-</sup> X(1) $\Sigma^+$  ground state with low-lying Th<sup>3+</sup>(6d)-O<sup>2-</sup> (1) $^2\Delta$ , (1) $^2\Pi$ , and (2) $^2\Sigma^+$  states.<sup>56</sup> Promotion of a 7s electron to the less polarizable 6d orbitals results in an increase in the bond length and decrease in the vibrational frequency. This suggests that both 7s and 6d are nonbonding, an inference that is supported by electronic structure calculations.

Our studies of ThO and ThO<sup>+</sup> have been discussed in earlier reviews.<sup>23,24</sup> The more recent work on ThF/ThF<sup>+</sup> has been motivated by interest in the electronic structures of the molecules, and the potential utility of ThF<sup>+</sup> as a species for studies of fundamental constants.<sup>58</sup> ThF<sup>+</sup> is isoelectronic with ThO and therefore is expected to have a low-energy (1) $^3\Delta_1$  state that could be used to probe the magnitude of the eEDM.<sup>17</sup> The potential advantages of using the ion are that it can be manipulated using external fields<sup>20</sup> and that the (1) $^3\Delta_1$  state was expected to be at an energy that is low enough to be easily populated.

Electronic transitions of ThF were located using both LIF and REMPI spectroscopy. The ground state was found to be  $|\Omega| = 1.5$ , as expected for the Th<sup>+</sup>(7s<sup>2</sup>6d)F<sup>-2</sup> $\Delta_{3/2}$  configuration. Dispersed fluorescence spectra yielded a ground state vibrational constant of approximately 605(15) cm<sup>-1</sup>, and a X(1) $^2\Delta_{5/2}$ -X(1) $^2\Delta_{3/2}$  spin-orbit interval of 2575(15) cm<sup>-1</sup>.

Theoretical calculations were used to predict the low-energy states of both ThF and ThF<sup>+</sup>. A 60 electron effective core potential, combined with a (27s,24p,18d,14f,6g,3h)/[13s,11p,10d,8f,6g,3h] contracted ANO valence basis set was used for Th (ECP60MWB\_ANO<sup>59,60</sup>). Dunning's aug-cc-pVTZ basis set<sup>34</sup> was used for F. The neutral molecule was examined using the CASSCF/MRCI+Q/SO sequence of methods. Molecular orbitals, derived from the CASSCF calculation, are shown in Figure 6. The HOMO-1 orbital

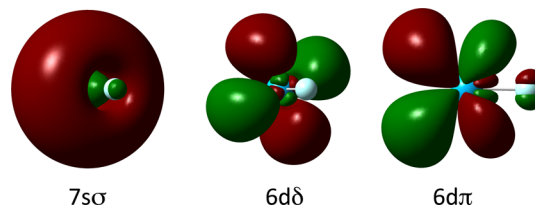


**Figure 6.** Isodensity surfaces ( $D = 0.02$ ) for the 7s, 6d $_\delta$ , and 6d $_\pi$  orbitals of ThF<sup>+</sup> calculated at the CASSCF level of theory.

was found to be a metal-centered 7s/6d $_\sigma$  hybrid, polarized away from the F<sup>-</sup> ligand, whereas the HOMO is predominantly atomic 6d $_\delta$ . The atomic character is preserved because the F atom does not have energetically accessible orbitals of  $\delta$  symmetry. However, Figure 6 shows that the 6d $_\pi$  orbital, which can mix with the ligand orbitals, has a rather modest antibonding interaction with F 2p $_\pi$  but retains most of its atomic character. CASSCF/MRCI+Q/SO calculations confirmed the X(1) $^2\Delta_{3/2}$  ground state assignment. The predicted harmonic vibrational frequency (574 cm<sup>-1</sup>) and spin-orbit interval  $^2\Delta_{5/2}$ - $^2\Delta_{3/2}$  (1939 cm<sup>-1</sup>) were underestimated. The error was modest for the vibration, but the calculated spin-orbit interaction was only 75% of the observed value.

Low-resolution PFI-ZEKE spectra for ThF revealed the presence of at least four electronically excited states of ThF<sup>+</sup> lying within 4000 cm<sup>-1</sup> of the first ionization threshold. The lowest energy excited state was found just 315 cm<sup>-1</sup> above the ground state zero-point level. As the 7s6d configuration in ThF<sup>+</sup> will be less strongly destabilized by F<sup>-</sup> (as compared to O<sup>2-</sup> in ThO), the 7s<sup>2</sup> (1) $\Sigma^+$  and 7s6d (1) $^3\Delta_1$  were expected to be very close in energy, such that either assignment for the ground state was viable. Attempts to achieve an unambiguous assignment from the PFI-ZEKE spectra were unsuccessful as the resolution was not sufficient to separate the  $J = 0$  and 1 levels (the (1) $\Sigma^+$  assignment would have been established by the identification of the  $J = 0$  level).<sup>58</sup> Surprisingly, the trends in molecular constants expected on the basis of LFT also failed to resolve the ambiguity. From the foregoing discussion, it would be expected that the (1) $^3\Delta_1$  state would have smaller rotational and vibrational constants than (1) $\Sigma^+$ . This behavior was followed by isoelectronic HfF<sup>+</sup> (ref 61), but the constants for the two lowest energy states of ThF<sup>+</sup> were quite similar (e.g., the harmonic vibrational constants for the first two states were 656.8(10) and 658.3(10) cm<sup>-1</sup>). Arguments based on relative band intensities favored the assignment of (1) $\Sigma^+$  as the ground state but were not conclusive. Since the publication of ref 58, we have obtained a well-resolved LIF spectrum of ThF<sup>+</sup> that shows an R(0) line (c.f. Figure 7), confirming that X(1) $\Sigma^+$  is the ground state.

Theoretical calculations were used to explore the question of why the (1) $\Sigma^+$  and (1) $^3\Delta_1$  states have such similar molecular constants. Multireference coupled-cluster (MRCC) calculations were carried out at the CCSD(T), CCSDT, and CCSDT(Q) levels of theory.<sup>58</sup> Spin-orbit interaction energies were included by using CASSCF wave functions to evaluate the spin-orbit matrix elements. The first two levels of theory predicted that (1) $^3\Delta_1$  was the ground state, whereas the calculation that included perturbative quadruple excitations gave (1) $\Sigma^+$  as the ground state. The difference between the vibrational constants for the (1) $\Sigma^+$  and (1) $^3\Delta_1$  states decreased with increasingly accurate recovery of the correlation energy.

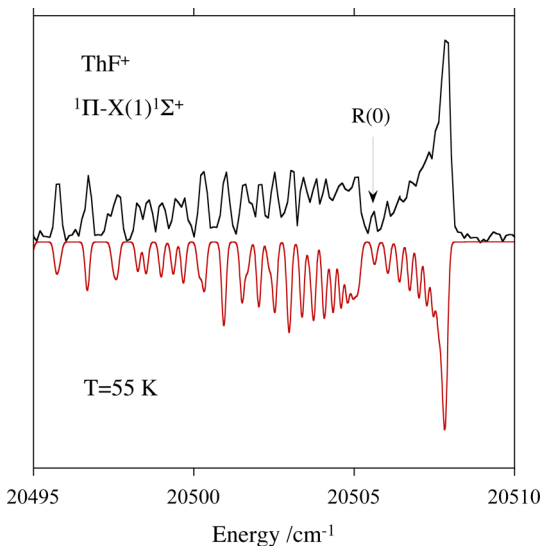


**Figure 7.** Laser-induced fluorescence spectrum of the [19.36]1-X(1) $^1\Sigma^+$ , 2-0 band of ThF $^+$ . The presence of the R(0) line confirms the  $^1\Sigma^+$  assignment for the ground state.

These results indicated that electron correlation was critical in determining the properties of the lowest energy states.

CASSCF/MRCI+Q/SO calculations for ThF $^+$ , reported here for the first time, yield an X(1) $^1\Sigma^+$  ground state, with the (1) $^3\Delta_1$  state at  $T_e = 187.5 \text{ cm}^{-1}$ . The experimental data are compared with the CASSCF/MRCI+Q/SO and MRCC results in Table 2. The similarity of the vibrational constants was not

**Table 2. Calculated and Observed Molecular Constants for ThF $^+$**

state/constant	MRCCSDT/ SO	MRCCSDT(Q)/ SO	MRCI +Q/SO	exp
(1) $^1\Sigma^+, T_e$ (cm $^{-1}$ )	143.3	0	0	0
(1) $^1\Sigma^+, \omega_e$ (cm $^{-1}$ )	663.6	659.8	665.9	656.8(10)
(1) $^1\Sigma^+, R_e$ (Å)	1.979	1.981	1.977	1.98(2)
(1) $^3\Delta_1, T_e$ (cm $^{-1}$ )	0	65.5	187.5	315.6(5)
(1) $^3\Delta_1, \omega_e$ (cm $^{-1}$ )	652.6	651.1	655.6	658.3(10)
(1) $^3\Delta_1, R_e$ (Å)	1.993	1.993	1.991	1.98(2)
(1) $^3\Delta_2, T_e$ (cm $^{-1}$ )	889.7	955.3	1055.5	1052.5(5)
(1) $^3\Delta_2, \omega_e$ (cm $^{-1}$ )	653.4	651.9	658.2	656.5(10)
(1) $^3\Delta_2, R_e$ (Å)	1.992	1.993	1.990	1.98(2)
(1) $^3\Delta_3, T_e$ (cm $^{-1}$ )	2157.1	2222.9	2152.8	3150(15)
(1) $^3\Delta_3, \omega_e$ (cm $^{-1}$ )	654.2	652.7	658.1	665(15)
(1) $^3\Delta_3, R_e$ (Å)	1.991	1.992	1.990	

fully reproduced by the former, which was comparable to the case for CCSDT in this respect. Eigenvectors from the CASSCF/MRCI+Q/SO calculations indicate that mixing of the 7s $^2$  and 7s6d  $^1\Sigma^+$  states, which is facilitated by their closeness in energy, is partly responsible for the similarity in the vibrational constants. Energies for the (1) $^3\Delta_1$  and (1) $^3\Delta_2$  states were predicted to be in reasonably good agreement with the experimental data, but the energy for (1) $^3\Delta_3$  was significantly underestimated (cf. Table 2). In this context it should be noted

that the (1) $^3\Delta_3$ –(1) $^3\Delta_1$  interval gives the most reliable reflection of the 6d $_\delta$  spin–orbit interaction. The relative energy of the (1) $^3\Delta_2$  component is complicated by the mutual repulsion of the 7s6d $_\delta$  (1) $^1\Delta_2$  and (1) $^3\Delta_2$  states. The measured ThF $^+$  (1) $^3\Delta_3$ –(1) $^3\Delta_1$  interval ( $2835(20) \text{ cm}^{-1}$ ) and ThF X(1) $^2\Delta_{5/2}$ –X(1) $^2\Delta_{3/2}$  interval ( $2575(15) \text{ cm}^{-1}$ ) should be reflective of the 6d $_\delta$  spin–orbit interaction. CASSCF/MRCI +Q/SO calculations underestimate both values by about 25%. In addition, the MRCC calculations for ThF $^+$  suffered from the same defect.

Predictions for higher-energy ThF $^+$  7s6d states that have not yet been observed are included in Table 3. These are provided as they may be useful for the design of experiments that involve the (1) $^3\Delta_1$  state. As this is not the ground state, population can be transferred into (1) $^3\Delta_1$  by stimulated emission pumping (as used to populate the (1) $^3\Delta_1$  state of ThO in the recent eEDM investigation<sup>19</sup>). Transition dipole moments, calculated at the ground state equilibrium distance, are presented in Table 3. The most favorable population transfer scheme would involve excitation of the (1) $^1\Pi_1 \leftarrow X(1)\Sigma^+$  transition followed by stimulated emission pumping of (1) $^1\Pi_1 \rightarrow (1)^3\Delta_1$ .

PFI-ZEKE measurements gave an IE for ThF of  $6.3953(4) \text{ eV}$ , which was just outside the range determined from electron impact measurements ( $6.0(3) \text{ eV}$ <sup>62</sup>). The updated value is greater than the IE of atomic Th, defining a difference between the bond dissociation energies of the neutral and the ion of  $D_0 - D_0^+ = 0.122 \text{ eV}$ . Despite this slight weakening of the bond on ionization, the vibrational and rotational constants for the ion were larger than those of the neutral molecule, indicating a reduced electrostatic repulsion near the equilibrium distance. This counterintuitive trend has been noted for other ThX/ThX $^+$  (refs 56 and 63) and HfX/HfX $^+$  (refs 26, 61, and 64) pairs.

**Spectroscopic and Theoretical Studies of ThS and ThS $^+$ .** The interactions of actinides with soft-donor ligands are of interest for the design of chelating ligands that may be used in separations schemes. As An–S bonds are expected to be less ionic than An–O bonds, they also provide an opportunity to observe a greater degree of covalency. Systematic DFT calculations for AnS/AnS $^+$  species were reported by Pereira et al.,<sup>65</sup> along with gas phase thermodynamic data derived from mass spectrometric measurements.

Electronic spectra for gas phase ThS were recently reported by Bartlett et al.<sup>63</sup> Consistent with DFT calculations and the electronic structure of ThO, the ground state was found to be Th(7s $^2$ )S X(1) $\Sigma^+$ . Several strong electronic transitions, all originating from the ground state and terminating on  $|\Delta\Omega| = 1$  excited states, were observed in the  $17\ 500$ – $24\ 000 \text{ cm}^{-1}$  energy range. Dispersed fluorescence spectra displayed a short progression of ground state vibrational levels ( $v'' = 0$ –3) ( $\omega_e'' = 479(1) \text{ cm}^{-1}$ ) and electronically excited states at  $3623(4)$  and  $4534(4) \text{ cm}^{-1}$  that were assigned to Th(7s6d $_\delta$ )S (1) $^3\Delta_1$  and (1) $^3\Delta_2$ . Due to the  $\Delta\Omega = 0, \pm 1$  optical selection rule, the (1) $^3\Delta_3$  component could not be observed in the laser-excited emission spectrum. The transitions to the (1) $^3\Delta$  states were about one-fourth the intensity of the transition back to X(1) $\Sigma^+$ , which indicates that the excited state had mixed singlet/triplet character.

The low-lying vibronic states of ThS $^+$  were characterized using two-color PFI-ZEKE measurements. Two vibronic progressions were observed at energies up to  $4000 \text{ cm}^{-1}$  above the ThS IE. These were assigned to the 7s X(1) $^2\Sigma^+$  ( $\omega_e'' = 517(2) \text{ cm}^{-1}$ ) and 6d $_\delta$  (1) $^2\Delta_{3/2}$  states ( $T_0 = 2136(3)$

**Table 3.** State Energies and Transition Dipole Moments for the Low-Energy States of  $\text{ThF}^+$ <sup>a</sup>

	$^1\Sigma^+$	$^3\Delta_1$	$^3\Delta_2$	$^3\Delta_3$	$^3\Pi_0$	$^3\Pi_1$	$^3\Pi_2$	$^1\Pi_1$	$^3\Sigma^+_1$
$^1\Sigma^+$	0	0.036	0.000	0.000	0.074	0.449	0.000	0.784	0.247
$^3\Delta_1$		202	0.051	0.000	0.449	0.075	0.006	0.169	0.001
$^3\Delta_2$			1047	0.058	0.000	0.353	0.033	0.270	0.072
$^3\Delta_3$				2163	0.000	0.000	0.440	0.000	0.000
$^3\Pi_0$					4930	0.014	0.000	0.075	0.296
$^3\Pi_1$						5254	0.009	0.051	0.349
$^3\Pi_2$							6418	0.015	0.000
$^1\Pi_1$								6827	0.156
$^3\Sigma^+_1$									8777

<sup>a</sup>These results are for MRCl+Q/SO calculations performed at an internuclear separation of 1.98 Å. The state energies in cm<sup>-1</sup> units are given by the numbers in italics. The transition moments are given in Debye units.

cm<sup>-1</sup>,  $\omega_e = 489(4)$  cm<sup>-1</sup>). Rotational resolution was not achieved, so assignments were based on the vibrational constants and comparison to theoretical calculations.

Low-lying states of ThS were predicted using CASSCF/MRCl+Q/SO calculations with the ECP60MWB\_ANO<sup>59,60</sup> (Th) and aug-cc-pVTZ (S)<sup>66</sup> basis sets. The ground state vibrational frequency, equilibrium bond length and the energies of the (1) $^3\Delta_1$  and (1) $^3\Delta_2$  states were all in good agreement with the experimental results. The previous DFT/B3LYP study<sup>65</sup> had yielded predictions for the ground state that were of almost the same quality. Ab initio electronic structure calculations showed that the ground state of ThS is distinctly less ionic than that of ThO. Near the equilibrium distance the leading contributions to the wave function were 56%  $\text{Th}^{2+}(7s^2)\text{S}^{2-}$  and 17%  $\text{Th}^+(7s^26d\pi)\text{S}^-(3p_\sigma^23p_\pi^3)$ . Similarly, the leading term for the (1) $^3\Delta$  state was only 74%  $\text{Th}^{2+}(7s5d_\delta)\text{S}^{2-}$ . These results suggest that an accurate treatment of the low-lying states may require the use of multireference methods, with the wider implication that single-reference methods may not be well suited for treatment of the interactions of actinides with soft-donor ligands. To examine the performance of another single-reference method, CCSD(T) calculations were carried out for ThS X(1) $^1\Sigma^+$ . Again, results were obtained that were in good agreement with the experimental observations. The value for the  $T_1$  diagnostic (0.025) implied that the molecule had non-negligible multireference character, but the validity of this test has been called into question for molecules that contain transition metals.<sup>67</sup> The reference state for the CCSD(T) calculation was generated by a Hartree–Fock (HF) calculation, and it was suggested that the high value for  $T_1$  may be a consequence of the HF determinant being a poor initial guess.<sup>68</sup> In support of this interpretation, CCSD(T) calculations that used the DFT/B3LYP determinant as the reference gave the same final results as the HF/CCSD(T) calculation, but the  $T_1$  diagnostic dropped to 0.016.

The permanent dipole moment of ThS X(1) $^1\Sigma^+$  is of interest as it provides a way of testing the charge separation. Clearly, the dipole moment should be quite sensitive to the degree to which the formal  $\text{Th}^{2+}\text{S}^{2-}$  and  $\text{Th}^+\text{S}^+$  configurations contribute to the wave function. The zero-point vibrationally averaged dipole moment for X(1) $^1\Sigma^+$  was determined using the data from the CASSCF/MRCl+Q ( $\langle \mu(R) \rangle_0^{\text{MRCl}} = 4.2$  D) and DFT/B3LYP ( $\langle \mu(R) \rangle_0^{\text{B3LYP}} = 4.4$  D) calculations. To test these predictions, the dipole moment was measured by means of the Stark effect on rotational lines of the {18.26}1-X(1) $^1\Sigma^+$  transition (experiments performed at the Arizona State University).<sup>69</sup> The value

obtained, 4.58(10) D, provided further evidence that a single-reference approach was applicable.

Although the ionic LFT model gives useful insights concerning the low-lying electronic states of ThO and ThS, the bonding includes considerable covalent contributions. Pyykkö et al.<sup>70</sup> have argued that these molecules can be viewed as having covalent triple bonds resulting from a  $\sigma^2\pi^4$  valence molecular orbital occupation. Our electronic structure calculations<sup>63</sup> agree with this configurational assignment, showing that the  $\sigma$  and  $\pi$  orbitals in question for ThS are formed by the Th 6d<sub>σ</sub> + S 3p<sub>σ</sub> and Th 6d<sub>π</sub> + S 3p<sub>π</sub> linear combinations, with approximately 75% contributions from the S 3p orbitals. In this context it is also of interest to note that the bonding orbitals included some Th 5f contributions, despite the relatively high energy of the 5f orbitals in the atomic limit. The percentage of 5f character was predicted to be 3.7 and 4.8% for the  $\pi$  and  $\sigma$  orbitals, respectively. Figure 8 shows the molecular orbitals.

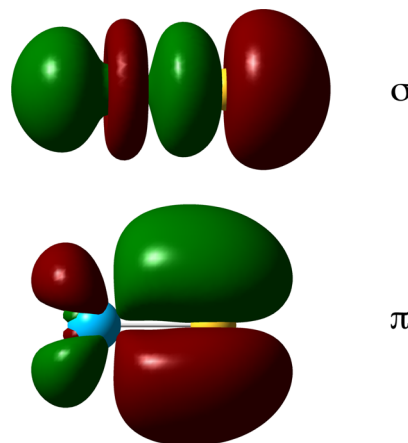


**Figure 8.** Isodensity surfaces ( $D = 0.02$ ) for  $\sigma$  (HOMO-1) and  $\pi$  (HOMO-2) bonding orbitals of ThS calculated at the CASSCF level of theory.

Consistent with this covalent picture of the bonding, the additive triple bond covalent radii proposed by Pyykkö et al.<sup>70</sup> predict ground state equilibrium bond lengths that are quite close to the measured values (1.89 vs 1.84 Å (exp) for ThO; 2.31 vs 2.34 Å (exp) for ThS).

CASSCF/MRCl+Q/SO calculations for ThS<sup>+</sup> yielded vibrational constants of 502 and 479 cm<sup>-1</sup> for the X(1) $^2\Sigma^+$  and (1) $^2\Delta_{3/2}$  states, reproducing the change expected from promotion of the 7s electron to 6d<sub>δ</sub>. The term energy predicted for (1) $^2\Delta_{3/2}$  (2499 cm<sup>-1</sup>) was also in acceptable agreement

with the spectroscopic data. As for the neutral molecule, the single-reference methods RCCSD(T) and DFT/B3LYP provided respectable predictions for the ground state. The ionization energy obtained from the PFI-ZEKE spectrum (6.7479(4) eV) was also recovered with reasonable accuracy by the CASSCF/MRCI+Q/SO (6.659 eV), RCCSD(T) (6.686 eV), and DFT/B3LYP (6.608 eV) calculations. Although the vibrational frequency for the ground state of the ion was 38 cm<sup>-1</sup> greater than that of the neutral molecule, the IE showed that the bond dissociation energy decreased by 0.44 eV on ionization.

**Spectroscopic and Theoretical Studies of ThN and ThN<sup>+</sup>.** The ThN/ThN<sup>+</sup> pair provides a model system for studies of actinide–nitrogen bonds. In addition, as ThN and ThO<sup>+</sup> are isoelectronic, comparisons of their low-energy states can yield further insights concerning the LFT view of the electronic structure.

Prior to the results reported here, the experimental data for ThN consisted of a gas phase determination of the bond dissociation energy (5.9(3) eV)<sup>71</sup> and measurements of the fundamental vibrational frequency for ThN isolated in a solid Ar matrix ( $\Delta G_{1/2}'' = 934.3$  cm<sup>-1</sup>).<sup>44</sup> DFT calculations for ThN,<sup>44</sup> performed to facilitate interpretation of the matrix data, yielded a X(1)<sup>2Σ<sup>+</sup> ground state with a fundamental vibrational frequency of  $\omega_e = 999$  cm<sup>-1</sup> and a bond length of  $R_e = 1.795$  Å. No data were available for ThN<sup>+</sup>.</sup>

In our experiments, gas phase ThN was produced by laser ablation of a Th target in the presence of a carrier gas flow that contained 0.05% NH<sub>3</sub> in He. LIF and REMPI spectra, recorded over the 19 700–21 200 cm<sup>-1</sup> range, exhibited a large number of optically active vibronic transitions. A low-resolution REMPI survey spectrum, recorded with mass selected detection of the ThN<sup>+</sup> ion, is shown in Figure 9. At least 20 distinct vibronic

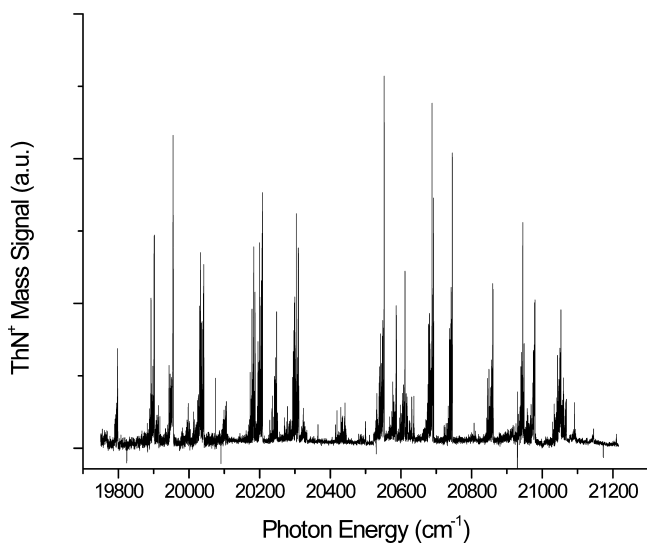


Figure 9. Low-resolution REMPI spectrum of ThN.

bands were observed within this 1500 cm<sup>-1</sup> interval. Rotationally resolved data were examined for several bands. Many of the structures were effected by local perturbations, which was not surprising given the density of states. A transition centered at 20 945 cm<sup>-1</sup> was found to be unperturbed (at a resolution of 0.06 cm<sup>-1</sup> fwhm). This band, and a simulation of the structure, is shown in Figure 10. Analysis confirmed the X(1)<sup>2Σ<sup>+</sup> assignment for the ground state, consistent with the expected</sup>

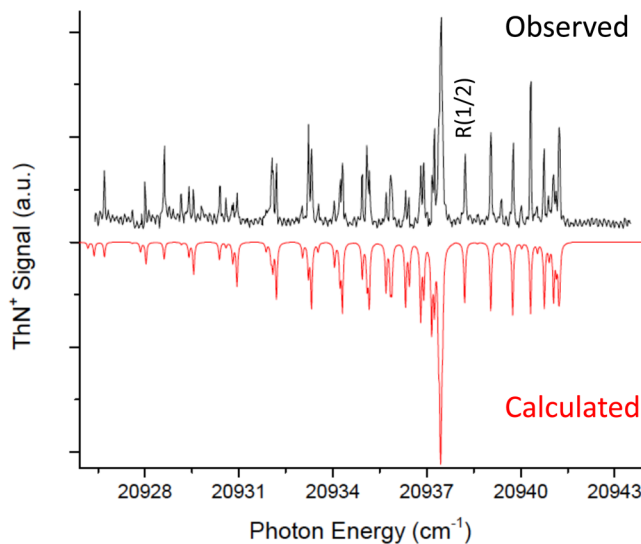


Figure 10. Rotationally resolved REMPI spectrum of ThN (upward-going trace). The lower trace is a simulation for a  $^2\Pi_{3/2}$ -X(1)<sup>2Σ<sup>+</sup> transition with a rotational temperature of 25 K.</sup>

Th(7s)N configuration. The transition was clearly  $^2\Pi$ -X(1)<sup>2Σ<sup>+</sup>, with the  $^2\Pi$  state being close to the Hund's case (a) or case (c) limit for spin-orbit coupling. The line positions could be adequately fit by assuming that the upper state was either the  $|\Omega| = 0.5$  or 1.5 component, but the intensity pattern was in better agreement with the assignment to  $|\Omega| = 1.5$ . Many of the lines in Figure 10 are closely spaced doublets, resulting from spin-rotation coupling in the ground state. Fitting to the line positions yielded a ground state rotational constant of  $B_0'' = 0.393(2)$  cm<sup>-1</sup> and a spin-rotation interaction constant of  $|\gamma_0'| = 0.017(3)$  cm<sup>-1</sup>. The former provided an estimate for the bond length of  $R_0 = 1.80(1)$  Å.</sup>

A dispersed fluorescence spectrum was obtained using excitation of a  $^2\Sigma^+-X(1)^2\Sigma^+$  band at 20 549 cm<sup>-1</sup>. Only two features were observed, corresponding to emission back to the  $v'' = 0$  and 1 levels of the ground state. A vibrational interval of  $\Delta G_{1/2}'' = 960(15)$  cm<sup>-1</sup> was defined by these bands. No other transitions were discernible for the range up to 5000 cm<sup>-1</sup> above the zero-point level, indicating that there were no excited  $^2\Sigma^+$  or  $^2\Pi$  states below this energy.

ThN and ThO<sup>+</sup> both have X(1)<sup>2Σ<sup>+</sup> ground states with similar bond lengths ( $R_0''(\text{ThO}^+) = 1.807$  Å) and vibrational frequencies ( $\Delta G_{1/2}''(\text{ThO}^+) = 950.0(1)$  cm<sup>-1</sup>). The first electronically excited states of ThO<sup>+</sup> are  $6d_\delta$  (1)<sup>2Δ<sub>3/2</sub> and (1)<sup>2Δ<sub>5/2</sub> at 2602 and 5852 cm<sup>-1</sup>. Due to the optical selection rules, the corresponding states of ThN would not appear in our dispersed fluorescence spectrum. ThO<sup>+</sup> has its lowest energy (1)<sup>2Π</sup> state at 9167 cm<sup>-1</sup>, which suggests that the corresponding state of ThN is probably above the range probed by the dispersed fluorescence spectrum.</sup></sup></sup>

It is also of interest to compare ThN with isoelectronic HfN. Ram and Bernath<sup>72</sup> analyzed a  $^2\Sigma^+-^2\Sigma^+$  band system for HfN that was recorded in emission near 6700 cm<sup>-1</sup>. Although the assignment was not conclusive, there was good evidence indicating that the lower state was the ground state. Molecular constants of  $\omega_e'' = 932.7164(15)$  cm<sup>-1</sup>,  $R_e'' = 1.724\ 678(36)$  Å, and  $\gamma_0'' = -0.054\ 57(19)$  cm<sup>-1</sup> were obtained for <sup>180</sup>HfN. The vibrational constants for ThN and HfN are, when scaled for the difference in the reduced masses, very similar. As both molecules are formally held together by triple bonds, it is

appropriate to make comparisons to the bond lengths predicted by Pyykkö et al.'s<sup>70</sup> covalent triple bond radii. For HfN the sum of the radii gives a bond length of 1.76 Å, which is reasonably close to the spectroscopic value. For ThN the sum gives 1.90 Å, which is overestimated by 0.1 Å. Part of the discrepancy might be traced to the repulsion between the N ligand and the Th 7s electron, but it would be surprising to find that an electron in the Th 7s orbital was subject to a stronger repulsion than an electron in the less polarizable Hf 6s orbital.

Electronic structure calculations for ThN were carried out using the CASSCF/MRCI+Q/SO sequence of methods. The basis sets were ECP60MWB\_ANO for Th and aug-cc-pVTZ for N.<sup>34</sup> Figure 11 shows the low-energy potential energy

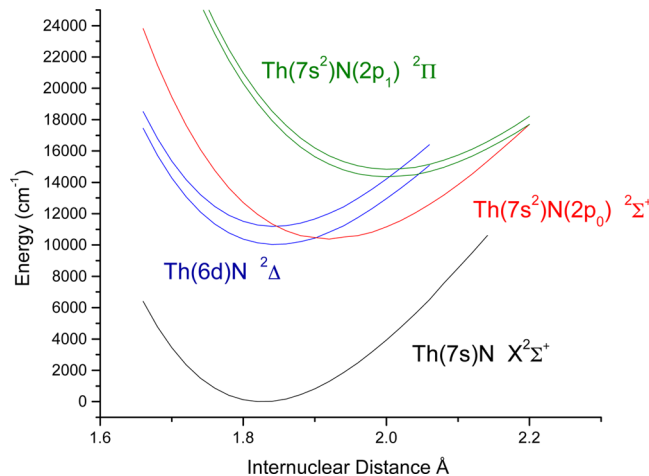


**Figure 11.** Calculated potential energy curves for the low-lying electronic states of ThN.

curves derived from these calculations. The  $X(1)^2\Sigma^+$  state was predicted to be well separated from the first electronically excited state ( $(1)^2\Delta_{3/2}$  at  $10\,015\text{ cm}^{-1}$ ). Calculated molecular constants for the ground state are presented along with the experimental results in Table 4. The  $(1)^2\Delta$  state was derived

**Table 4. Observed and Calculated Ground State Constants for ThN/ThN<sup>+</sup>**

constant	B3LYP	CCSD(T)	MRCI+Q	exp
$\omega_e\text{ (cm}^{-1}\text{)}$	989.1	946.0	941.3	
$\omega_e x_e\text{ (cm}^{-1}\text{)}$	3.3	3.5	3.4	
$\Delta G_{1/2}\text{ (cm}^{-1}\text{)}$	982.5	939.0	934.5	950(15)
$R_e\text{ (\AA)}$	1.806	1.787	1.826	
$B_0\text{ (cm}^{-1}\text{)}$	0.391	0.393	0.382	0.393(2)
IE (cm <sup>-1</sup> )	50970	50476	46097	51032(3)
$\Delta G_{1/2}^+\text{ (cm}^{-1}\text{)}$	1053.9	1008.8	1003.8	1010.0(5)
$B_0^+\text{ (cm}^{-1}\text{)}$	0.407	0.400	0.3981	0.410(5)

from the Th 6d<sub>5</sub> configuration, whereas the low-energy  $(2)^2\Sigma^+$  and  $(1)^2\Pi$  states arise from the promotion of an electron from the  $\sigma$  or  $\pi$  bonding orbitals to Th 7s (e.g.,  $(2)^2\Sigma^+$  has the configuration  $\sigma\pi^4\text{ }7s^2$ ). When UN was compared with UO<sup>+</sup>, it was noted that the stronger electrostatic interactions in the nitride produced a greater destabilization of the 5f and 6d orbitals. The greater relative destabilization of 6d in ThN, as compared to ThO<sup>+</sup>, is evident in the upward shift of 6d<sub>5</sub>  $(1)^2\Delta_{3/2}$  by approximately 7400 cm<sup>-1</sup>.

Spectra for ThN<sup>+</sup> were taken using the PFI-ZEKE technique. A low-resolution scan located the IE and the  $v'' = 1$  level of the ground state. These were the only molecular ion features appearing within 1400 cm<sup>-1</sup> of the ionization threshold. A rotationally resolved spectrum for the  $v'' = 0$  level is shown in Figure 12. This trace yielded an IE of 6.3272(4) eV and a

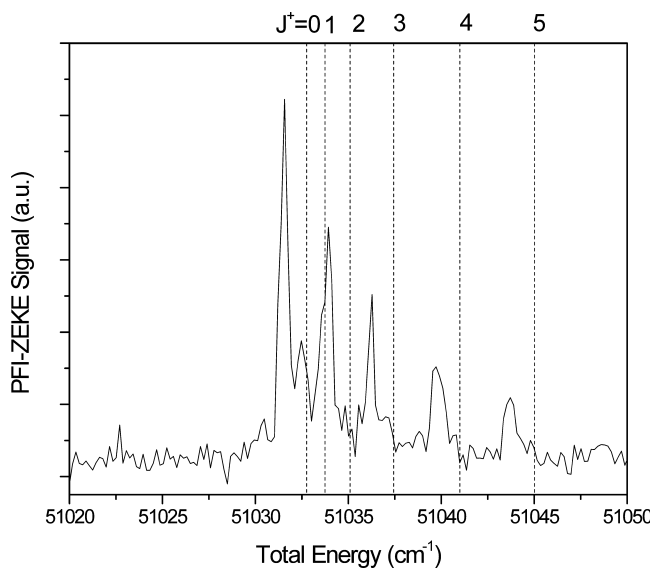


**Figure 12.** Rotationally resolved PFI-ZEKE spectrum for the  $X(1)^1\Sigma^+$ ,  $v = 0$  level of ThN<sup>+</sup>.

rotational constant of  $B_0'' = 0.410(5)\text{ cm}^{-1}$ . A well-resolved  $J = 0$  feature was present, confirming that the ground state is  $X(1)^1\Sigma^+$  resulting from the removal of the 7s electron. The electrostatic repulsion of the 7s electron was reflected by the contraction of the internuclear distance ( $\Delta R_0'' = -0.04\text{ \AA}$ ) and an increase in the vibrational frequency ( $\Delta(\Delta G_{1/2}) = 50(15)\text{ cm}^{-1}$ ) on ionization. The IE for ThN differs from that of Th by just 0.02 eV.

Theoretical calculations for ThN<sup>+</sup> were carried out using the same methods as described above for ThN, and the potential energy curves are plotted in Figure 13. The molecular constants

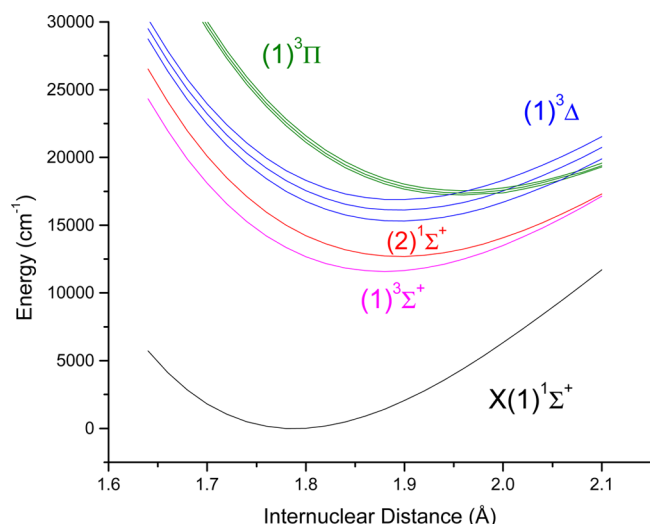


**Figure 13.** Calculated potential energy curves for the low-lying electronic states of ThN<sup>+</sup>.

derived from the ground state potential are listed in Table 4. As the  $\sigma$ -bonding orbital is the HOMO for  $\text{ThN}^+$ , the first excited state is  $(1)^3\Sigma^+$ , obtained by promotion of a  $\sigma$ -electron to Th 7s. The associated  $(2)^1\Sigma^+$  state is very close in energy. Promotion of a  $\sigma$ -electron to Th 6d<sub>5</sub> produces the  $(1)^3\Delta$  manifold. Due to the transfer of an electron from a bonding orbital and the shorter internuclear distance of  $\text{ThN}^+$ , the  $(1)^3\Delta_1$  state is at a significantly higher energy ( $15\ 234\ \text{cm}^{-1}$ ) than the related  $(6d_5 \leftarrow 7s)\ (1)^2\Delta_{3/2}$  state of  $\text{ThN}$  ( $10\ 015\ \text{cm}^{-1}$ ). The calculations place the  $(1)^3\Pi$  state, resulting from the  $7s \leftarrow \pi$ -bonding promotion, just above the  $(1)^3\Delta$  states. Many transitions from the bonding orbitals to the Th 6d, 7p, and 5f orbitals are expected at higher energies. For  $\text{ThN}$ , the tiers of doublet and quartet states originating from these configurations readily account for the density of vibronic states seen in Figure 9.

Multireference methods were used for  $\text{ThN}/\text{ThN}^+$  to include excited states that are subject to spin-orbit interactions. However, as noted in the Introduction, we are also interested in evaluating the quality of low-cost computational methods for the prediction of ground state properties. Single-reference calculations were carried out using the CCSD(T) and DFT/B3LYP methods with the basis sets specified above. The molecular constants from these calculations, listed in Table 4, were obtained by fitting the Morse potential function to a series of 13 single-point energies computed near the equilibrium distance. Both electronic structure methods yielded respectable results. As for  $\text{ThS}$ , the CCSD(T) calculations for  $\text{ThN}$  yielded moderately high values for the  $T_1$  (0.026) and  $D_1$  (0.064) diagnostics. This was slightly surprising as the MRCI calculations indicated that the ground state is dominated by the  $\text{Th}(7s)\text{N}$  configuration. In contrast to the situation for  $\text{ThS}$ , using the DFT/B3LYP determinant for the reference did little to reduce the values of the diagnostics. Despite these cautionary flags, the single-reference methods did appear to be quite reliable. In addition to recovering the molecular constants, the single-reference methods provided reliable predictions for the IE. Useful information for the lowest energy excited states, which differ in symmetry from the ground state, could also be obtained. For example, DFT/B3LYP predicts an energy of  $9878\ \text{cm}^{-1}$  for the  $(1)^2\Delta$  state (spin-free) with an equilibrium bond length of  $1.825\ \text{\AA}$ .

Further experimental studies of  $\text{ThN}/\text{ThN}^+$  are in progress, but the preliminary results reported here show that the main qualitative features of the electronic structure can be anticipated using a combination of simple molecular orbital and LFT models.

## SUMMARY AND OUTLOOK

The application of conventional laser spectroscopy techniques to gas phase actinide diatomics provides definitive insights concerning electronic structure and bonding. In the examples described here, we have found that the complex patterns of low-lying electronic states for these molecules can be rationalized using LFT models and reasonably well predicted using high-level ab initio electronic structure calculations. It is usually assumed that the early actinides will have the greatest propensity for involvement of the 5f electrons in covalent bonding. For simple Th and U diatomics, experimentally validated electronic structure calculations do indicate a small fraction of 5f character in the bonding orbitals. However, for U compounds the predominantly atomic character of 5f is unmistakably reflected by the atomic-like patterns of low-lying states (this is most probably true for Th as well, but we

have not yet observed transitions to the 5f states). This supports the continued use of traditional LFT models as a way to anticipate the electronic structure. As the 5f orbitals contract with increasing atomic number, LFT predictions are expected to be even more closely followed by the transuranic actinides.

Theoretical modeling of larger actinide-containing molecules must rely on lower-level, computationally efficient methods such DFT. Our initial tests of the reliability of this approach, based on comparisons with the experimental data for the diatomics, show that DFT is an adequate model for actinide bonds in most instances. The only exception encountered in our work has been  $\text{ThF}^+$ , where the interactions between two nearly degenerate electronic configurations present a severe challenge.

To date our research has been focused on a few compounds of Th and U. For the diatomics, future studies of hydrides, carbides, phosphides, and chlorides are of obvious interest. Gas phase samples of all of these species may be generated using laser ablation techniques,<sup>24</sup> and the metal-centered electronic transitions will be well-suited for LIF, REMPI, and PFI-ZEKE measurements. Our work has been carried out in a laboratory that is not equipped to handle samples that pose radiation hazards greater than those associated with small quantities of  $^{232}\text{Th}$  or  $^{238}\text{U}$ . Similar studies of compounds of Np, Pu, and Am would certainly be viable in a suitably configured facility.

Two-photon ionization methods provide IE measurements that are orders of magnitude more accurate than the electron impact and photoelectron spectroscopy techniques that have been used in the past. A problem with the earlier techniques was that gas phase samples of the molecules of interest were generated using high-temperature furnaces. This often resulted in significant thermal population of electronically excited states, so that threshold ionization measurements reflected ionization from the excited states. The two-photon PFI-ZEKE technique described here has the advantage that initial and final quantum states of the neutral molecule and the ion can be selected.

Accurate data for IE's are of value in their own right, but they also facilitate the determination of bond dissociation energies for neutral molecules. Collision-induced dissociation is an excellent tool for the determination of bond dissociation energies of molecular ions, but it is not suitable for neutral molecules. However, if the IEs of the molecule and the metal atom are known, this information can be combined with the bond dissociation energy of the ion to determine that of the neutral molecule.

Metal–metal bonding for the actinides can be examined in detail using the metal dimers. Spectroscopic data for  $\text{An}_2$  have yet to be reported, but there have been theoretical studies of these molecules. Gagliardi and Roos<sup>73</sup> found that  $\text{U}_2$  should possess a weak quintuple bond ( $D_e = 9275\ \text{cm}^{-1}$ )<sup>74</sup> with orbital angular momentum of  $\Lambda = 11$  and total spin of  $S = 3$ . A systematic study of the homonuclear dimers  $\text{Ac}_2$ ,  $\text{Th}_2$ ,  $\text{Pa}_2$ , and  $\text{U}_2$  indicated that  $\text{Pa}_2$  has the strongest bond ( $32\ 300\ \text{cm}^{-1}$ ), but  $\text{Th}_2$  is quite stable ( $D_e = 26\ 500\ \text{cm}^{-1}$ ).<sup>74</sup> The  $\text{Th}_2$  and  $\text{U}_2$  dimers have been produced in our laser ablation source and detected by mass spectrometry. However, initial attempts to record REMPI spectra have yielded structureless signals. This is probably due to the high densities of electronically excited states and the possible contributions to the dimer ion mass channel by fragments from larger clusters. Given these difficulties, it seems that near-threshold anion photodetachment spectroscopy<sup>75,76</sup> would be a better method for  $\text{An}_2$  studies.

This allows for mass selection prior photodetachment and probing of the lowest energy states of the dimers.

Moving to larger molecules, triatomic actinide species (with one actinide atom) are suitable for investigation using the techniques described here.  $\text{UO}_2$  and the  $\text{UO}_2^+$  cation have been characterized and both exhibit complex vibronic structures. The density of bound states for  $\text{UO}_2$ , at energies above the ionization limit, is so high that the molecule exhibits delayed ionization.<sup>37</sup> The interactions of actinides with organic ligands is a topic of both fundamental and practical interest. Studies of Th and U atoms interacting with classical ligands such as acetylene, cyclopentadienyl, benzene, and cyclooctatetraene would facilitate our understanding of the organometallic chemistry of the actinides. In this context, the pioneering work of Yang and co-workers is noteworthy. Using one-photon PFI-ZEKE techniques, they have explored the structures of a large number of organometallic lanthanide species.<sup>77–80</sup> Their methods should be equally successful when applied to organometallic actinides.

For larger molecules the ground state structures and bonding are of primary interest, and one-photon PFI-ZEKE measurements can provide this information for ionic species. Another successful spectroscopic technique for gas phase ligated actinide ions, advanced by Groenewold, Van Stipdonk, and co-workers, uses electrospray ion production with IR multiphoton dissociation to characterize ground state vibrational transitions.<sup>81–85</sup> Studies of ligated neutral atoms should be feasible using anion photodetachment spectroscopy.

Gas phase spectroscopic experiments for the actinides are providing critical data for the evaluation and further development of computational models. The work carried out to date has demonstrated the feasibility of applying laser spectroscopic tools to studies of actinide compounds, and the range of properties that can be determined accurately. There is every reason to expect rapid progress resulting from studies of the prototypical species listed above, and the indispensable interplay between theory and experiment.

## AUTHOR INFORMATION

### Corresponding Author

\*M. C. Heaven. E-mail: mheaven@emory.edu. Phone: 404 727 6617. FAX 404 727 6586.

### Notes

The authors declare no competing financial interest.

### Biographies



Michael C. Heaven received his B.Sc. in Chemistry in 1975 and his Ph.D. in Physical Chemistry in 1979, both from the Queen Mary

College, University of London. After postdoctoral studies at the University of London, England, and Bell Laboratories, Murray Hill, NJ, from 1979–1982, he became an Assistant Professor at the Department of Chemistry, Illinois Institute of Technology, Chicago. In 1986, he joined the Department of Chemistry, Emory University, as Associate Professor and was promoted to Professor in 1992. From 1996–1998, he was Director of Graduate Studies and from 2003–2009 Associate Chair of the Department of Chemistry, Emory University. His research interests include the electronic spectroscopy of transient intermediates, energy transfer kinetics, intermolecular forces, and unimolecular decay dynamics.



Beau J. Barker is currently a Seaborg postdoctoral fellow at Los Alamos National Laboratory investigating luminescence and resonant non-radiative energy transfer in actinyl containing complexes. He obtained a B.A. degree in chemistry from Gustavus Adolphus College in St. Peter, MN. He has an M.S. degree in computational chemistry from the University of Minnesota—Duluth and a Ph.D. degree from the University of Minnesota—Twin Cities under the guidance of Doreen Leopold. He was a postdoctoral fellow with Michael Heaven at Emory University where he was introduced to the exciting world of actinide chemistry.



Ivan O. Antonov received his undergraduate degree in chemistry from Samara State University in Russia in 2002. He worked as a research assistant at the Samara Branch of the Lebedev Physical Institute until 2005 and then joined the Ph.D. program at Emory University in Atlanta, GA, where he studied the spectroscopy of actinide-containing molecules with Prof. Michael Heaven. Since receiving his Ph.D. in 2013, he has worked as a postdoctoral fellow at Sandia National Laboratories in Livermore, CA.

## ACKNOWLEDGMENTS

We gratefully acknowledge the support of this research by the Department of Energy under grant DE-FG02-01ER15153. The

electronic structure calculations reported here were carried out using the resources of the Cherry Emerson Center for Scientific Computation, which is supported by the NSF MRI-R2 grant CHE-0958205.

## ■ REFERENCES

- (1) Morss, L. R. In *Chemistry of the Actinide and Transactinide Elements*, 4th ed.; 6 vols. edited by Morss, Lester R., Edelstein, Norman M., Fuger, Jean, Katz, Joseph J., Eds. Springer: Dordrecht, The Netherlands, 2010; Vol. 46, pp 1562–1563.
- (2) Runde, W.; Neu, M. P. Actinides in the geosphere. In *The chemistry of the actinide and transactinide elements*; Morss, L.R., Edelstein, N.M., Fuger, J., Eds.; Springer: Dordrecht, The Netherlands, 2010; pp 3475–3593.
- (3) Dolg, M.; Cao, X. Relativistic Pseudopotentials: Their Development and Scope of Applications. *Chem. Rev.* **2012**, *112*, 403–480.
- (4) Weigand, A.; Cao, X.; Hangele, T.; Dolg, M. Relativistic Small-Core Pseudopotentials for Actinium, Thorium, and Protactinium. *J. Phys. Chem. A* **2014**, *118*, 2519–2530.
- (5) Pyykkö, P.; Stoll, H. Relativistic pseudopotential calculations, 1993–June 1999. *Chem. Model.* **2000**, *1*, 239–305.
- (6) Vukovic, S.; Hay, B. P. De Novo Structure-Based Design of Bis-amidoxime Uranophiles. *Inorg. Chem.* **2013**, *52*, 7805–7810.
- (7) Averkiev, B. B.; Mantina, M.; Valero, R.; Infante, I.; Kovacs, A.; Truhlar, D. G.; Gagliardi, L. How accurate are electronic structure methods for actinoid chemistry? *Theor. Chem. Acc.* **2011**, *129*, 657–666.
- (8) Gagliardi, L. The study of actinide chemistry with multiconfigurational quantum chemical methods. *Int. J. Quantum Chem.* **2011**, *111*, 3302–3306.
- (9) Dolg, M.; Cao, X. Computational methods: lanthanides and actinides. *Comput. Inorg. Bioinorg. Chem.* **2009**, *503*–515.
- (10) Fleig, T.; Olsen, J.; Visscher, L. The generalized active space concept for the relativistic treatment of electron correlation. II. Large-scale configuration interaction implementation based on relativistic 2- and 4-spinors and its application. *J. Chem. Phys.* **2003**, *119*, 2963–2971.
- (11) Pyykkö, P. Recent developments in the theory of f-element molecules. *Inorg. Chim. Acta* **1987**, *139*, 243–245.
- (12) Pyykkö, P. Relativistic effects in chemistry: More common than you thought. *Annu. Rev. Phys. Chem.* **2012**, *63*, 45–64.
- (13) Neidig, M. L.; Clark, D. L.; Martin, R. L. Covalency in f-element complexes. *Coord. Chem. Rev.* **2013**, *257*, 394–406.
- (14) Kaledin, L. A.; McCord, J. E.; Heaven, M. C. Laser spectroscopy of UO: characterization and assignment of states in the 0- to 3-eV Range, with a comparison to the electronic structure of ThO. *J. Mol. Spectrosc.* **1994**, *164*, 27–65.
- (15) Han, J.; Goncharov, V.; Kaledin, L. A.; Komissarov, A. V.; Heaven, M. C. Electronic spectroscopy and ionization potential of UO<sub>2</sub> in the gas phase. *J. Chem. Phys.* **2004**, *120*, 5155–5163.
- (16) Field, R. W. Diatomic molecular electronic structure beyond simple molecular constants. *Ber. Bunsen-Ges. Phys. Chem.* **1982**, *86*, 771–779.
- (17) Meyer, E. R.; Bohn, J. L. Prospects for an electron electric-dipole moment search in metastable ThO and ThF<sup>+</sup>. *Phys. Rev. A At., Mol., Opt. Phys.* **2008**, *78*, 010502/010501–010502/010504.
- (18) Fleig, T.; Nayak, M. K. Electron electric dipole moment and hyperfine interaction constants for ThO. *J. Mol. Spectrosc.* **2014**, *300*, 16–21.
- (19) Baron, J.; Campbell, W. C.; DeMille, D.; Doyle, J. M.; Gabrielse, G.; Gurevich, Y. V.; Hess, P. W.; Hutzler, N. R.; Kirilov, E.; Kozyryev, I.; O’Leary, B. R.; Panda, C. D.; Parsons, M. F.; Petrik, E. S.; Spaun, B.; Vutha, A. C.; West, A. D. Order of Magnitude Smaller Limit on the Electric Dipole Moment of the Electron. *Science* **2014**, *343*, 269–272.
- (20) Loh, H.; Cossel, K. C.; Grau, M. C.; Ni, K. K.; Meyer, E. R.; Bohn, J. L.; Ye, J.; Cornell, E. A. Precision Spectroscopy of Polarized Molecules in an Ion Trap. *Science* **2013**, *342*, 1220–1222.
- (21) Meyer, E. R.; Bohn, J. L. Prospects for an electron electric-dipole moment search in metastable ThO and ThF<sup>+</sup>. *Phys. Rev. A: At., Mol., Opt. Phys.* **2008**, *78*, 010502/010501–010502/010504.
- (22) Orzel, C. Searching for new physics through atomic, molecular and optical precision measurements. *Phys. Scr.* **2012**, *86*, 068101 068109..
- (23) Heaven, M. C. Probing actinide electronic structure using fluorescence and multi-photon ionization spectroscopy. *Phys. Chem. Chem. Phys.* **2006**, *8*, 4497–4509.
- (24) Heaven, M. C.; Gibson, J. K.; Marcalo, J. Molecular spectroscopy and reactions of the actinides in the gas phase and cryogenic matrices. In *The chemistry of the actinide and transactinide elements*; Morss, L. R., Edelstein, N. M., Fuger, J., Eds.; Springer: Dordrecht, The Netherlands, 2010; pp 4079–4156.
- (25) Schlag, E. W. *ZEKE Spectroscopy*; Cambridge University Press: Cambridge, England, 1998.
- (26) Merritt, J. M.; Bondybey, V. E.; Heaven, M. C. Ionization energy measurements and spectroscopy of HfO and HfO<sup>+</sup>. *J. Chem. Phys.* **2009**, *130*, 144503/144501–144503/144509.
- (27) Goncharov, V.; Kaledin, L. A.; Heaven, M. C. Probing the electronic structure of UO<sup>+</sup> with high-resolution photoelectron spectroscopy. *J. Chem. Phys.* **2006**, *125*, 133202/133201–133202/133208.
- (28) Antonov, I. O.; Heaven, M. C. Spectroscopic and Theoretical Investigations of UF and UF<sup>+</sup>. *J. Phys. Chem. A* **2013**, *117*, 9684–9694.
- (29) Krauss, M.; Stevens, W. J. Electronic structure of uranium hydride (UH), uranium fluoride (UF), and their ions. *J. Comput. Chem.* **1983**, *4*, 127–135.
- (30) Fedorov, D. G.; Nakajima, T.; Hirao, K. An ab initio study of U and UF. *J. Chem. Phys.* **2003**, *118*, 4970.
- (31) Pantazis, D. A.; Neese, F. All-Electron Scalar Relativistic Basis Sets for the Actinides. *J. Chem. Theory Comput.* **2011**, *7*, 677–684.
- (32) Peralta, J. E.; Batista, E. R.; Scuseria, G. E.; Martin, R. L. All-Electron Hybrid Density Functional Calculations on UF<sub>n</sub> and UCl<sub>n</sub> (n = 1–6). *J. Chem. Theory Comput.* **2005**, *1*, 612–616.
- (33) Dolg, M.; Cao, X. Accurate Relativistic Small-Core Pseudopotentials for Actinides. Energy Adjustment for Uranium and First Applications to Uranium Hydride. *J. Phys. Chem. A* **2009**, *113*, 12573–12581.
- (34) Dunning, T. H., Jr. Gaussian basis sets for use in correlated molecular calculations. I. The atoms boron through neon and hydrogen. *J. Chem. Phys.* **1989**, *90*, 1007–1023.
- (35) Werner, H.-J.; Knowles, P. J.; Lindh, R.; Manby, F. R.; Schütz, M.; et al. *MOLPRO*, version 2010, a package of ab initio programs, <http://www.molpro.net/>.
- (36) Linton, C.; Adam, A. G.; Steimle, T. C. Stark and Zeeman effect in the [18.6]3.5 - X(1)4.5 transition of uranium monofluoride, UF. *J. Chem. Phys.* **2014**, *140*, 214305/214301–214305/214307.
- (37) Merritt, J. M.; Han, J.; Heaven, M. C. Spectroscopy of the UO<sub>2</sub><sup>+</sup> cation and the delayed ionization of UO<sub>2</sub>. *J. Chem. Phys.* **2008**, *128*, 084304/084301–084304/084308.
- (38) Kaledin, L. A.; Heaven, M. C. Electronic spectroscopy of UO. *J. Mol. Spectrosc.* **1997**, *185*, 1–7.
- (39) Heaven, M. C.; Goncharov, V.; Steimle, T. C.; Ma, T.; Linton, C. The permanent electric dipole moments and magnetic g factors of uranium monoxide. *J. Chem. Phys.* **2006**, *125*, 204314/204311–204314/204311.
- (40) Hildenbrand, D. L.; Lau, K. H. Redetermination of the thermochemistry of gaseous uranium fluorides (UF<sub>5</sub>, UF<sub>2</sub>, and UF). *J. Chem. Phys.* **1991**, *94*, 1420–1425.
- (41) Matthew, D. J.; Morse, M. D. Resonant two-photon ionization spectroscopy of jet-cooled UN: Determination of the ground state. *J. Chem. Phys.* **2013**, *138*, 184303/184301–184303/184307.
- (42) Pepper, M.; Bursten, B. E. The electronic structure of actinide-containing molecules: a challenge to applied quantum chemistry. *Chem. Rev.* **1991**, *91*, 719–741.
- (43) Gabelnick, S. D.; Reedy, G. T.; Chasanov, M. G. Infrared spectra and structure of some matrix-isolated lanthanide and actinide oxides. *J. Chem. Phys.* **1974**, *60*, 1167–1171.

- (44) Kushto, G. P.; Souter, P. F.; Andrews, L. An infrared spectroscopic and quasirelativistic theoretical study of the coordination and activation of dinitrogen by thorium and uranium atoms. *J. Chem. Phys.* **1998**, *108*, 7121–7130.
- (45) Souter, P. F.; Kushto, G. P.; Andrews, L.; Neurock, M. Experimental and Theoretical Evidence for the Isolation of Thorium Hydride Molecules in Argon Matrices. *J. Phys. Chem. A* **1997**, *101*, 1287–1291.
- (46) Edvinsson, G.; Lagerqvist, A. Rotational analysis of yellow and near infrared bands in thorium(II) oxide. *Phys. Scr.* **1984**, *30*, 309–320.
- (47) Edvinsson, G.; Lagerqvist, A. Rotational analysis of two red band systems in the thorium oxide (ThO) spectrum. *Phys. Scr.* **1985**, *32*, 602–610.
- (48) Edvinsson, G.; Lagerqvist, A. A low-lying  $\Omega = 2$  state in the thorium monoxide (ThO) molecule. *J. Mol. Spectrosc.* **1985**, *113*, 93–104.
- (49) Edvinsson, G.; Lagerqvist, A. Rotational analysis of some violet and green bands in the thorium oxide (ThO) spectrum. *J. Mol. Spectrosc.* **1987**, *122*, 428–439.
- (50) Edvinsson, G.; Lagerqvist, A. Two band systems of thorium oxide (ThO) in the near ultraviolet. *J. Mol. Spectrosc.* **1988**, *128*, 117–125.
- (51) Edvinsson, G.; Lagerqvist, A. Two new band systems in thorium oxide (ThO). *Phys. Scr.* **1990**, *41*, 316–320.
- (52) Dewberry, C. T.; Etchison, K. C.; Grubbs, G. S.; Powoski, R. A.; Serafin, M. M.; Peebles, S. A.; Cooke, S. A. Oxygen-17 hyperfine structures in the pure rotational spectra of SrO, SnO, BaO, HfO and ThO. *Phys. Chem. Chem. Phys.* **2007**, *9*, 5897–5901.
- (53) Dewberry, C. T.; Etchison, K. C.; Cooke, S. A. The pure rotational spectrum of the actinide-containing compound thorium monoxide. *Phys. Chem. Chem. Phys.* **2007**, *9*, 4895–4897.
- (54) Wang, F.; Le, A.; Steimle, T. C.; Heaven, M. C. Communication: The permanent electric dipole moment of thorium monoxide, ThO. *J. Chem. Phys.* **2011**, *134*, 031102/031101–031102/031103.
- (55) Vutha, A. C.; Spaun, B.; Gurevich, Y. V.; Hutzler, N. R.; Kirilov, E.; Doyle, J. M.; Gabrielse, G.; DeMille, D. Magnetic and electric dipole moments of the H  $^3\Delta_1$  state in ThO. *Phys. Rev. A At., Mol., Opt. Phys.* **2011**, *84*, 034502/034501–034502/034504.
- (56) Goncharov, V.; Heaven, M. C. Spectroscopy of the ground and low-lying excited states of ThO $^+$ . *J. Chem. Phys.* **2006**, *124*, 064312/064311–064312/064317.
- (57) Goncharov, V.; Han, J.; Kaledin, L. A.; Heaven, M. C. Ionization energy measurements and electronic spectra for ThO. *J. Chem. Phys.* **2005**, *122*, 204311/204311–204311/204316.
- (58) Barker, B. J.; Antonov, I. O.; Heaven, M. C.; Peterson, K. A. Spectroscopic investigations of ThF and ThF $^+$ . *J. Chem. Phys.* **2012**, *136*, 104305/104301–104305/104309.
- (59) Cao, X.; Dolg, M. Segmented contraction scheme for small-core actinide pseudopotential basis sets. *THEOCHEM* **2004**, *673*, 203–209.
- (60) Cao, X.; Dolg, M.; Stoll, H. Valence basis sets for relativistic energy-consistent small-core actinide pseudopotentials. *J. Chem. Phys.* **2003**, *118*, 487–496.
- (61) Barker, B. J.; Antonov, I. O.; Bondybey, V. E.; Heaven, M. C. Communication: Spectroscopic measurements for Hff $^+$  of relevance to the investigation of fundamental constants. *J. Chem. Phys.* **2011**, *134*, 201102/201101–201102/201104.
- (62) Lau, K. H.; Brittain, R. D.; Hildenbrand, D. L. High temperature thermodynamic studies of some gaseous thorium fluorides. *J. Chem. Phys.* **1989**, *90*, 1158–1164.
- (63) Bartlett, J. H.; Antonov, I. O.; Heaven, M. C. Spectroscopic and Theoretical Investigations of ThS and ThS $^+$ . *J. Phys. Chem. A* **2013**, *117*, 12042–12048.
- (64) Barker, B. J.; Antonov, I. O.; Heaven, M. C. Low-lying states of Hfs $^+$  and the ionization energy of Hfs. *J. Mol. Spectrosc.* **2012**, *275*, 35–40.
- (65) Pereira, C. C. L.; Marsden, C. J.; Marcalo, J.; Gibson, J. K. Actinide sulfides in the gas phase: experimental and theoretical studies of the thermochemistry of AnS (An = Ac, Th, Pa, U, Np, Pu, Am and Cm). *Phys. Chem. Chem. Phys.* **2011**, *13*, 12940–12958.
- (66) Woon, D. E.; Dunning, T. H., Jr. Gaussian basis sets for use in correlated molecular calculations. III. The atoms aluminum through argon. *J. Chem. Phys.* **1993**, *98*, 1358–1371.
- (67) Jiang, W.; DeYonker, N. J.; Wilson, A. K. Multireference Character for 3d Transition-Metal-Containing Molecules. *J. Chem. Theory Comput.* **2012**, *8*, 460–468.
- (68) Evangelisti, F. Personal communication, April 2014.
- (69) Le, A.; Heaven, M. C.; Steimle, T. C. The permanent electric dipole moment of thorium sulfide, ThS. *J. Chem. Phys.* **2014**, *140*, 024307/024301–024307/024305.
- (70) Pyykkö, P.; Riedel, S.; Patzschke, M. Triple-bond covalent radii. *Chem.—Eur. J.* **2005**, *11*, 3511.
- (71) Gingerich, K. A. Gaseous metal nitrides. III. On the dissociation energy of thorium mononitride and predicted dissociation energies of diatomic Group III–VI transition-metal nitrides. *J. Chem. Phys.* **1968**, *49*, 19–24.
- (72) Ram, R. S.; Bernath, P. F. Fourier transform infrared emission spectroscopy of the [6.7] $^2\Sigma^+ - \chi^2\Sigma^+$  system of HfN. *J. Mol. Spectrosc.* **1997**, *184*, 401–412.
- (73) Gagliardi, L.; Roos, B. O. Quantum chemical calculations show that the uranium molecule U<sub>2</sub> has a quintuple bond. *Nature* **2005**, *433*, 848–851.
- (74) Roos, B. O.; Malmqvist, P.-A.; Gagliardi, L. Exploring the actinide–actinide bond: Theoretical studies of the chemical bond in Ac<sub>2</sub>, Th<sub>2</sub>, Pa<sub>2</sub> and U<sub>2</sub>. *J. Am. Chem. Soc.* **2006**, *128*, 17000.
- (75) Neumark, D. M. Probing chemical dynamics with negative ions. *J. Chem. Phys.* **2006**, *125*, 132303/132301–132303/132315.
- (76) Neumark, D. M. Slow Electron Velocity-Map Imaging of Negative Ions: Applications to Spectroscopy and Dynamics. *J. Phys. Chem. A* **2008**, *112*, 13287–13301.
- (77) Yang, D.-S. High-Resolution Electron Spectroscopy of Gas-Phase Metal-Aromatic Complexes. *J. Phys. Chem. Lett.* **2011**, *2*, 25–33.
- (78) Lei, Y.; Wu, L.; Sohnlein, B. R.; Yang, D.-S. High-spin electronic states of lanthanide-arene complexes: Nd(benzene) and Nd-(naphthalene). *J. Chem. Phys.* **2012**, *136*, 204311/204311–204311/204318.
- (79) Liu, Y.; Kumari, S.; Roudjane, M.; Li, S.; Yang, D.-S. Electronic states and pseudo Jahn-Teller distortion of heavy metal-monobenzene complexes: M(C<sub>6</sub>H<sub>6</sub>) (M = Y, La, and Lu). *J. Chem. Phys.* **2012**, *136*, 134310/134311–134310/134319.
- (80) Kumari, S.; Roudjane, M.; Hewage, D.; Liu, Y.; Yang, D.-S. High-resolution electron spectroscopy of lanthanide (Ce, Pr, and Nd) complexes of cyclooctatetraene: The role of 4f electrons. *J. Chem. Phys.* **2013**, *138*, 164307/164301–164307/164309.
- (81) Groenewold, G. S.; van Stipdonk, M. J.; Oomens, J.; de Jong, W. A.; McIlwain, M. E. The gas-phase bis-uranyl nitrate complex [(UO<sub>2</sub>)<sub>2</sub>(NO<sub>3</sub>)<sub>5</sub>] $^-$ : Infrared spectrum and structure. *Int. J. Mass Spectrom.* **2011**, *308*, 175–180.
- (82) Gresham, G. L.; Dinescu, A.; Benson, M. T.; Van Stipdonk, M. J.; Groenewold, G. S. Investigation of Uranyl Nitrate Ion Pairs Complexed with Amide Ligands Using Electrospray Ionization Ion Trap Mass Spectrometry and Density Functional Theory. *J. Phys. Chem. A* **2011**, *115*, 3497–3508.
- (83) Groenewold, G. S.; van Stipdonk, M. J.; Oomens, J.; de Jong, W. A.; Gresham, G. L.; McIlwain, M. E. Vibrational spectra of discrete UO<sub>2</sub> $^{2+}$  halide complexes in the gas phase. *Int. J. Mass Spectrom.* **2010**, *297*, 67–75.
- (84) Groenewold, G. S.; Van Stipdonk, M. J.; de Jong, W. A.; Oomens, J.; Gresham, G. L.; McIlwain, M. E.; Gao, D.; Siboulet, B.; Visscher, L.; Kullman, M.; Polfer, N. Infrared spectroscopy of dioxouranium(V) complexes with solvent molecules: effect of reduction. *ChemPhysChem* **2008**, *9*, 1278–1285.
- (85) Groenewold, G. S.; Oomens, J.; de Jong, W. A.; Gresham, G. L.; McIlwain, M. E.; Van Stipdonk, M. J. Vibrational spectroscopy of anionic nitrate complexes of UO<sub>2</sub> $^{2+}$  and Eu $^{3+}$  isolated in the gas phase. *Phys. Chem. Chem. Phys.* **2008**, *10*, 1192–1202.

**■ NOTE ADDED IN PROOF**

It should be noted that the first spectroscopic observation of ThS was that of Liang and Andrews (Matrix Infrared Spectra and Quasirelativistic DFT Studies of ThS and ThS<sub>2</sub>. *J. Phys. Chem. A* **2002**, *106*, 4038–4041).